An updated parameterization for infrared emission and absorption by water vapor in the National Center for Atmospheric Research Community Atmosphere Model

William D. Collins, Jeremy K. Hackney, and David P. Edwards
National Center for Atmospheric Research, Boulder, Colorado, USA

Received 5 October 2001; revised 1 April 2002; accepted 7 April 2002; published 30 November 2002.

[1] An updated parameterization for the absorption and emission of infrared radiation by water vapor has been developed for the Community Atmosphere Model (CAM) from the National Center for Atmospheric Research (NCAR). The CAM is the latest version of the NCAR Community Climate Model (CCM). This updated treatment preserves the formulation of the radiative transfer equations using the absorptivity/emissivity method. However, the components of the absorptivity and emissivity related to water vapor have been replaced with new terms calculated with the General Line-by-line Atmospheric Transmittance and Radiance Model (GENLN2). The mean absolute errors in the surface and top-of-atmosphere clear-sky longwave fluxes for standard atmospheres are reduced to less than 1 W/m^2. Mean absolute differences between the cooling rates from the original method and GENLN2 are typically 0.2 K/d. These differences are reduced by at least a factor of 3 using the updated parameterization. The updated parameterization increases the longwave cooling at 300 mbar by 0.4 to 0.7 K/d, and it decreases the cooling near 800 mbar by 0.2 to 0.6 K/d. The increased cooling is caused by line absorption and the foreign continuum in the rotation band, and the decreased cooling is caused by the self-continuum in the rotation band. These changes in the vertical profile of longwave cooling interact strongly with the parameterization of convection. The effects on the fluxes, diabatic cooling rates, and climate state are illustrated using simulations with the new climate model. *INDEX TERMS:* 3337 Meteorology and Atmospheric Dynamics: Numerical modeling and data assimilation; 3319 Meteorology and Atmospheric Dynamics: General circulation; 3359 Meteorology and Atmospheric Dynamics: Radiative processes; *KEYWORDS:* radiative transfer, water vapor, continuum, GCM, longwave cooling

Citation: Collins, W. D., J. K. Hackney, and D. P. Edwards, An updated parameterization for infrared emission and absorption by water vapor in the National Center for Atmospheric Research Community Atmosphere Model, *J. Geophys. Res.*, *107*(D22), 4664, doi:10.1029/2001JD001365, 2002.

1. Introduction

[2] In the present-day climate, H_2O contributes approximately 60% of the atmospheric greenhouse effect [*Kiehl and Trenberth*, 1997]. In addition, roughly 77% of the warming from doubling CO_2 results from the water vapor feedback in the climate system [*Ramanathan*, 1981; *Rind et al.*, 1991]. For these reasons, it is essential to treat the interaction of terrestrial thermal radiation with H_2O as accurately as possible in general circulation models (GCMs). Thermal radiation interacts both with quantum transitions of the water vapor molecule known as lines and with a structureless absorption known as the water vapor continuum. The continuum is modeled as the sum of far-wing line extinction. Several studies have demonstrated that the longwave cooling rates and thermodynamic state simulated by GCMs are sensitive to the treatment of water vapor line strengths [*Pinnock and Shine*, 1998] and the continuum [*Schwarzkopf and Ramaswamy*, 1999; *Zhong and Haigh*, 1999].

[3] The Community Atmosphere Model (CAM) is the latest GCM developed by the National Center for Atmospheric Research (NCAR). The CAM is based upon the Community Climate Model (CCM) [*Kiehl et al.*, 1996, 1998a], a GCM widely used in the international climate community. In all versions of CCM since CCM1, the treatment of thermal absorption and emission by H_2O has been the original formulation developed by *Ramanathan and Downey* [1986]. There have been substantial changes in both the spectral data for H_2O lines and the formulation of the continuum since this parameterization was developed. Several studies have documented biases in the modeled clear-sky longwave fluxes relative to observations that can be traced directly to the H_2O parameterization [e.g., *Lubin and Harper*, 1996; *Pinto et al.*, 1997; *Briegleb and Bromwich*, 1998]. In addition, the clear-sky longwave cooling rates show persistent differences relative to modern line-by-

0148-0227/02/2001JD001365

line and band models [*Iacono et al.*, 2000]. In order to improve the accuracy of the fluxes computed by CCM, the authors have developed an updated parameterization for the longwave absorption and emission by water vapor.

[4] This updated formulation replaces just the parameterizations for absorption and emission of thermal radiation by H_2O in CAM. The only other difference in the radiative flux calculations between CCM and CAM is the general treatment of geometrical cloud overlap [*Collins*, 2001]. We have retained the explicit and separate dependence upon the emission and path temperatures first introduced in the original scheme. The main differences between the original and updated parameterizations are related to line and continuum absorption by H_2O. In the original scheme, the effects of lines are modeled using a Malkmus band model in the limit of strong line absorption. Self-broadening of lines is not included. The continuum is treated following the approach of *Roberts et al.* [1976] in the wave number range 500–1200 cm^{-1}. In the updated scheme, the effects of lines are calculated using current data on line parameters without parametric fitting to the Malkmus model. Self-broadening and foreign line broadening are explicitly incorporated. The self- and foreign-broadened water vapor continuum are treated following *Clough et al.* [1989] for the entire thermal infrared spectrum.

[5] The effects of the updated formulation are qualitatively similar to the results of *Zhong and Haigh* [1999], *Schwarzkopf and Ramaswamy* [1999], and *Iacono et al.* [2000]. *Iacono et al.* [2000] introduce a correlated-k code with modern line and continuum physics into the NCAR CCM. They attribute most of the differences between the radiative fluxes, heating rates, and climate state from the original and modified CCM to the change in the H_2O continuum. However, we show that there are also substantial changes in the cooling by rotation lines in the upper troposphere when the model is made consistent with modern line-by-line calculations. Both *Zhong and Haigh* [1995] and the authors of this study modify their respective wide-band radiation model using GENLN and demonstrate its accuracy relative to line-by-line models. The effects found by *Zhong and Haigh* [1999], *Iacono et al.* [2000], and this investigation show that updating the line and continuum absorption results in increased longwave cooling in the upper troposphere and reduced cooling in the lower and middle troposphere. All three model studies show that the effects of these changes cool the upper troposphere, warm the lower troposphere, and dry the lower and middle troposphere over the tropics and midlatitudes. The consistency among the three sets of results suggests that these effects may be a general consequence of improvements in the treatment of H_2O radiative properties.

[6] The formulation of the updated parameterization is described in section 2. Fluxes and cooling rates computed with the original and updated parameterizations are compared against benchmark line-by-line calculations in section 3. The biases in the original parameterization are decomposed in terms of line and continuum absorption for various parts of the thermal spectrum. Time-mean fluxes and cooling rates computed with the original and updated parameterizations in the full climate model are compared in section 4. The response of the climate model to the updated parameterization, and the changes in other physical processes required to recover a realistic mean state, are discussed in section 5. The advantages of the updated approach and future developments in the radiative parameterizations for CAM are outlined in section 6. The need for additional observations of spectral absorption in the far infrared is discussed in the context of the response of the climate model to changes in continuum absorption.

2. Method for Calculating Absorptivity and Emissivity

2.1. Formulation of Radiative Transfer

[7] In previous versions of the Community Climate Model, the equations of infrared radiative transfer have been formulated in terms of absorptivity and emissivity [*Manabe and Möller*, 1961]. This approach is retained in the current Community Atmospheric Model. In the absorptivity/emissivity method, infrared scattering by cirrus particles is neglected. The diffusivity approximation is substituted for the angular integrals in the expressions for the upwelling and downwelling fluxes. The downwelling flux at the top interface of the model is assumed to be identically zero, and the surface is assumed to radiate at an effective black-body temperature of T_0. With these simplifications, the equations for the longwave fluxes are [*Ramanathan and Downey*, 1986]:

$$F^{\downarrow}(z) = B(T_\infty)E(z,z_\infty) - \int_z^{z_\infty} A(z,z')\frac{dB(z')}{dz'}dz' \qquad (1)$$

$$F^{\uparrow}(z) = B(T_0) + \int_0^{z} A(z,z')\frac{dB(z')}{dz'}dz' \qquad (2)$$

The symbols in these equations are defined in Table 1. The absorption and emission of thermal radiation by water vapor and radiatively active trace gases are represented by $A(z, z')$ and $E(z, z')$, respectively.

[8] The absorption and emission of thermal radiation affects the subsequent evolution of the climate model by altering the diabatic cooling of the atmosphere. The cooling is calculated for each layer in the vertical discretization of the atmosphere. For a layer between the altitudes of z_i and z_{i+1}, the diabatic cooling related to thermal radiation is

$$Q = \frac{g}{c_p}\frac{\left[F^{\uparrow}(z_{i+1}) - F^{\downarrow}(z_{i+1})\right] - \left[F^{\uparrow}(z_i) - F^{\downarrow}(z_i)\right]}{p_{i+1} - p_i} \qquad [K/s] \quad (3)$$

Additional symbols are defined in Table 1.

[9] The terms $A(z, z')$ and $E(z, z')$ include the effects of thermal radiation interacting with discrete quantum transitions, known as lines, and with a structureless continuum. For wave numbers less than 1000 cm^{-1}, the lines are associated with rotational states of the H_2O molecule. For wave numbers greater than 1200 cm^{-1}, the lines are associated with rotational-vibrational states. In intermediate wave numbers between 800 and 1200 cm^{-1}, the line absorption is several orders of magnitude less than the adjacent rotational and rotational-vibrational bands. This spectral interval is known as the atmospheric window, where the effect of the continuum is very important. The interaction of radiation with each line is a complex function

Table 1. Definition of Terms in Fluxes

Term	Definition	Units
$F^{\downarrow}(z)$	downwelling infrared flux at altitude z above surface	W/m^2
$F^{\uparrow}(z)$	upwelling infrared flux at altitude z above surface	W/m^2
Q	infrared heating rate	K/s
T_0	temperature at surface	K
T_∞	temperature at top of model	K
z_∞	altitude at top of model	m
$B(T)$	Stefan-Boltzmann emission at temperature T	W/m^2
$B(z)$	Stefan-Boltzmann emission at temperature $T(z)$	W/m^2
$A(z, z')$	Absorptivity between altitudes z and z'	–
$E(z, z')$	Emissivity between altitudes z and z'	–
g	Gravitational acceleration	m/s^2
c_p	Specific heat at constant pressure	$Jkg^{-1}K^{-1}$
p_i	Atmospheric pressure at altitude z_i	$N\,m^{-2}$

of the local thermodynamic state and the spectral distribution of the radiation. The difficulty in computing $A(z, z')$ and $E(z, z')$ is compounded by the thousands of lines of water vapor in the thermal infrared and by the dependence of these terms on the atmospheric structure between z and z'.

[10] For these reasons, A and E are not computed from first principles in general circulation models. Instead, A and E are estimated using a three-step process. First, A and E are calculated for a wide variety of homogeneous atmospheric conditions using a line-by-line (LBL) radiative model. LBL codes compute the effects of the lines and continua at very high spectral resolution. The pre-computed A and E are then loaded into the general circulation model either as tables or as nonlinear multi-parameter functions fit to the tables. Second, the vertically stratified atmosphere between two arbitrary altitudes z and z' is replaced by an equivalent homogeneous atmosphere. The thermodynamic properties of the homogeneous atmosphere are chosen to approximate the absorption and emission of the stratified atmosphere as closely as possible [*Goody and Yung*, 1989]. The use of this equivalence eliminates the need to pre-compute A and E over the enormous parameter space of vertical atmospheric structure. Finally, the A and E for the equivalent homogeneous atmosphere are interpolated from the tables or estimated from the functional fits.

[11] The three steps are discussed in the subsequent sections. The line-by-line model is described in section 2.2, the equivalence between inhomogeneous and homogeneous atmospheres is described in section 2.3, and the calculation of the tables is discussed in section 2.4.

2.2. Line-by-Line Model

[12] The updated method is based upon calculations from the General Line-by-line Atmospheric Transmittance and Radiance Model (GENLN2 v.4) [*Edwards*, 1992]. In the 6.3-μm band, radiances computed with GENLN2 compare well with other line-by-line codes [*Soden et al.*, 2000]. In the current version of GENLN2, the parameters for H_2O lines have been obtained from the HITRAN-96 data base [*Rothman et al.*, 1998], and the continuum is treated with the Clough, Kneizys, and Davies (CKD) model version 2.1 [*Clough et al.*, 1989]. The GENLN calculations do not include the effects of recent revisions to the line parameters [*Rothman*, 2000] and recent improvements in the CKD continuum following *Han et al.* [1997] and *Tobin et al.* [1999]. (Note that heating rate calculations with CKD 2.4 suggest that CKD 2.1 overestimates the differences relative to Roberts (D. Kratz, private communication, 2002)). To generate the absorptivity and emissivity, GENLN is used to calculate the transmission through homogeneous atmospheres for H_2O lines alone and for H_2O lines and continuum. The fluxes and cooling rates calculated from the CAM longwave code for five standard atmospheres [*Anderson et al.*, 1986] are then evaluated using GENLN calculations for the same atmospheres.

2.3. Formulation of Absorptivity and Emissivity

2.3.1. Treatment of Line Absorption

[13] The absorption and emission of thermal radiation by water vapor lines along an atmospheric path are governed by the spectral distribution of the radiation, the pressure p, the specific humidity $q(p)$, and the atmospheric temperature $T(p)$ along the path. Consider a spectral band containing N spectral lines with transition wave numbers ν_i and absorption coefficients $k_i(\nu, T, p, q)$:

$$k_i(\nu, T, p, q) = S_i(T) f(\nu, \nu_i, T, p, q) \qquad \left[1/\left(cm^{-1}.g.cm^{-2}\right)\right] \tag{4}$$

The factor $S_i(T)$ is the line strength for line i. The factor $f(\nu, \nu_i, T, p, q)$ is a dimensionless line shape, a function of wave number ν with its maximum value at $\nu = \nu_i$. The line shape depends upon q because of self-line-broadening. The characteristic width of the line shape at a reference pressure p_0 and specific humidity q_0 is $\alpha_i(T)$. The absorptance for radiation in the spectral band propagating between layers at pressures p_1 and p_2 is determined by the H_2O path:

$$W = \int_{p_1}^{p_2} dW(p) \qquad \left[g/cm^2\right]$$
$$W(p) = q(p)dp/g \tag{5}$$

The absorptance over some wave number interval ν_1 to ν_2 is given by:

$$A_l = 1 - \int_{\nu_1}^{\nu_2} \exp\left[-\sum_{i=1}^{N} \int_{p_1}^{p_2} k_i(\nu, T, p, q) dW(p)\right] d\nu \tag{6}$$

[14] Scaling theory is a relationship between an inhomogeneous path and an equivalent homogeneous path with nearly identical line absorption (equation (6)) for the spectral band under consideration [*Goody and Yung*, 1989]. As discussed in section 2.1, scaling theory is used to reduce the parameter space of atmospheric conditions that have to be evaluated. The equivalent pressure, temperature, and absorber amount are calculated using the standard Curtis-Godson scaling theory for absorption lines [*Curtis*, 1952; *Godson*, 1953]. In addition, we retain explicit dependence on the emission temperature of the radiation following *Ramanathan and Downey* [1986], and we introduce dependence on an equivalent relative humidity. These five parameters are summarized in Table 2 and derived below. In the following derivations, a tilde denotes a parameter derived using scaling theory for the equivalence between homogeneous and inhomogeneous atmospheres. The subscript b denotes a parameter which depends upon the spectral band under consideration.

Table 2. Independent Parameters in A and E

Parameter[a]	Definition	Units	Equation	Effects
T_e	Emission temperature of radiation	K	–	Spectral distribution of radiation
$\widetilde{T_b}$	Air temperature	K	(7)	Line strength (from partition function); collision broadened line width; self- and foreign continuum temperature dependence
$\widetilde{P_b}$	Air pressure	Nm^{-2}	(9)	Foreign collision broadening of lines; foreign continuum absorption coefficient
$\widetilde{U_b}$, U'	Pressure-weighted precipitable water	gcm^{-2}	(13), (29)	Optical depth of lines continuum
$\tilde{\rho}$	Relative humidity	–	(14)	Self-broadened line width; self-continuum absorption coefficient

[a] A tilde denotes a parameter derived using scaling theory for the equivalence between homogeneous and inhomogeneous atmospheres. The subscript b denotes a parameter which depends upon the spectral band under consideration.

[15] The absorber-weighted path temperature is:

$$\widetilde{T_p} = \frac{1}{W}\int_{p_1}^{p_2} T(p)dW(p) \tag{7}$$

The H_2O path and pressure for a homogeneous atmosphere with equivalent line absorption are [*Goody and Yung*, 1989]

$$\widetilde{W_b} = \int_{p_1}^{p_2} \frac{\phi_b(T)}{\phi_b\left(\widetilde{T_p}\right)} dW(p) \tag{8}$$

$$\widetilde{P_b} = \frac{1}{\widetilde{W_b}}\int_{p_1}^{p_2} \frac{\psi_b(T)}{\psi_b\left(\widetilde{T_p}\right)} pdW(p) \tag{9}$$

where

$$\phi_b(T) = \sum_{i=1}^{N} S_i(T) \tag{10}$$

$$\psi_b(T) = \left\{\sum_{i=1}^{N} [S_i(T)\alpha_i(T)]^{1/2}\right\}^2 \tag{11}$$

It is convenient to calculate the absorptance in terms of a pressure-weighted H_2O path

$$U = \int_{p_1}^{p_2} \frac{p}{p_0} dW(p) \tag{12}$$

The equivalent pressure-weighted H_2O path is simply

$$\widetilde{U_b} = \frac{\widetilde{P_b}}{p_0}\widetilde{W_b} \tag{13}$$

[16] Although the relative humidity (or H_2O vapor pressure) is not included in standard Curtis-Godson scaling theory, it should be treated explicitly as an independent variable. The vapor pressure determines the self-broadening of lines and the strength of the self-continuum. The effective relative humidity $\widetilde{\rho}$ is defined in terms of an effective H_2O specific humidity $\widetilde{q_s}$ and saturation specific humidity $\widetilde{q_s}$ along the path:

$$\widetilde{\rho} = \frac{\widetilde{q}}{\widetilde{q_s}} \tag{14}$$

$$\widetilde{q} = \frac{g\ W}{p_2 - p_1} \tag{15}$$

$$\widetilde{q_s} = \frac{\epsilon e_s\left(\widetilde{T_p}\right)}{\widetilde{P} - (1-\epsilon)e_s\left(\widetilde{T_p}\right)} \tag{16}$$

$$\widetilde{P} = \frac{p_0 U}{W} \tag{17}$$

where $e_s(T)$ is the saturation vapor pressure at temperature T, $\widetilde{P}$ is an effective pressure, and $\epsilon = 0.622$ is the ratio of gas constants for air and water vapor. The effective vapor pressure is by definition:

$$\widetilde{e} = \frac{\widetilde{q}\widetilde{P}}{\epsilon + (1-\epsilon)\widetilde{q}} \tag{18}$$

2.3.2. Treatment of Continuum Absorption

[17] It is important to insure that the scaling theory for lines preserves the amount of continuum absorption along the inhomogeneous path. The CKD continuum absorption coefficient has the form

$$k_c(\nu, T, e, p) = k(\nu, T)\left(\frac{e}{p_0}C_s(\nu, T) + \frac{(p-e)}{p_0}C_f(\nu)\right) \cdot\left[1/\left(cm^{-1}.g.cm^{-2}\right)\right] \tag{19}$$

Here e is the vapor pressure of H_2O, $C_s(\nu, T)$ is the self-continuum coefficient, and $C_f(\nu)$ is the foreign continuum coefficient. Temperature dependence for the foreign continuum coefficient has been omitted in the absence of adequate laboratory measurements. In addition, theoretical calculations and field data suggest that the dependence is weak [*Tobin et al.*, 1999]. The prefactor $k(\nu, T)$ has a much weaker temperature dependence than $C_s(\nu, T)$. The continuum absorption in a wave number interval ν_1 to ν_2 is

$$A_c = 1 - \int_{\nu_1}^{\nu_2} \exp\left[-\int_{p_1}^{p_2} k_c(\nu, T, e, P)dW(p)\right]d_\nu \tag{20}$$

After application of the scaling theory for lines, the continuum absorption in the equivalent homogeneous atmosphere is:

$$\widetilde{A_c} = 1 - \int_{\nu_1}^{\nu_2} \exp\left[-k_c\left(\nu, \widetilde{T_p}, \widetilde{e}, \widetilde{P_b}\right)W\right]d_\nu \tag{21}$$

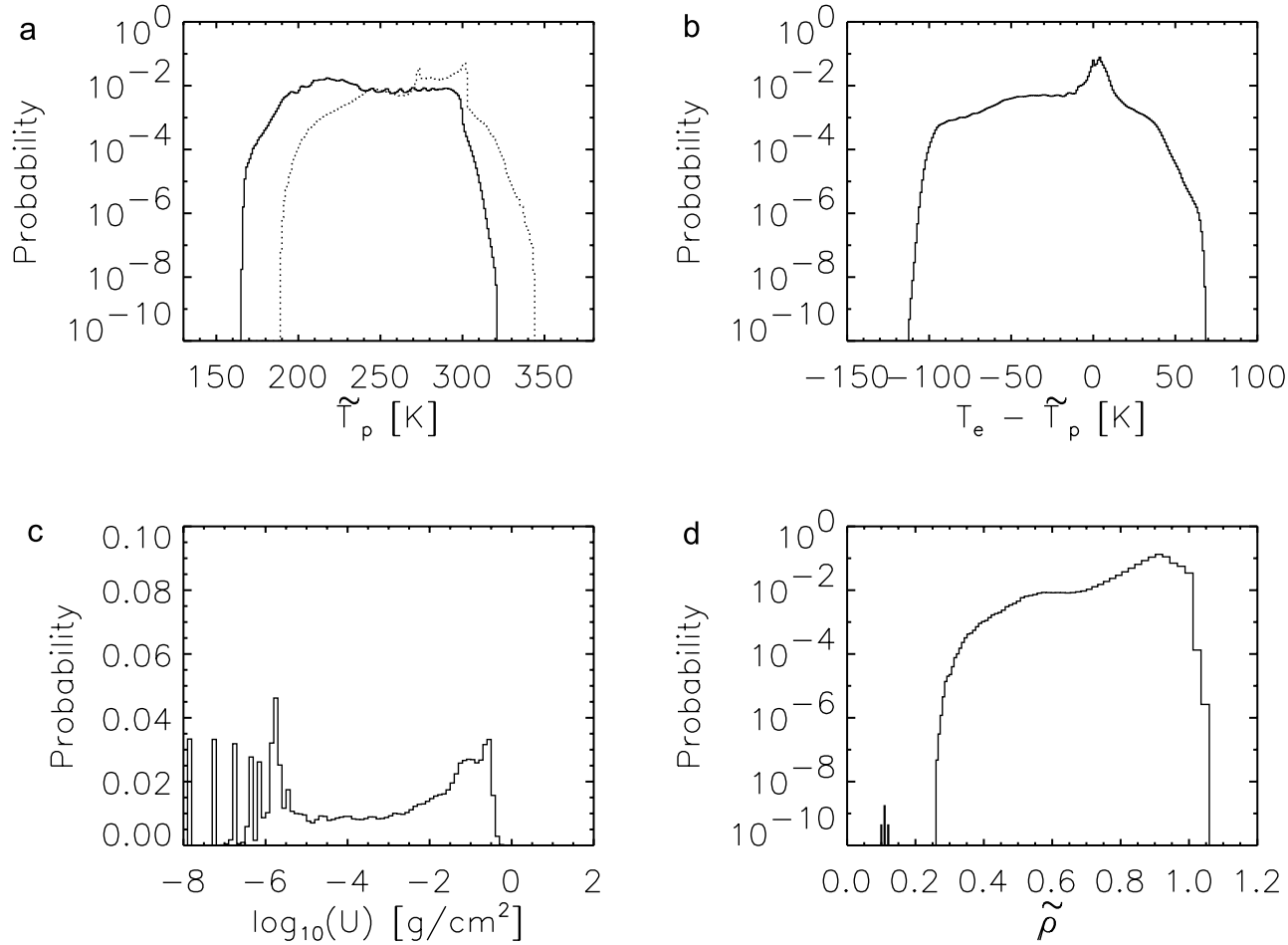

Figure 1. Probability distributions of atmospheric parameters given in Table 2. (a) Path temperature; (b) difference between emission and path temperature; (c) pressure-weighted water vapor path; and (d) relative humidity with respect to water vapor saturation. In Figure 1a, the surface temperature distribution is plotted as a dotted line. The distributions are obtained from instantaneous hourly values from a global 400-day simulation of CAM under present-day conditions.

The issue is whether $A_c \simeq \widetilde{A}_c$ in the rotation, rotation-vibration, and window bands.

[18] Outside the midinfrared window (the so-called non-window region), the H_2O continuum is dominated by the foreign component [*Clough et al.*, 1992]. Therefore the self-continuum terms in k_c (equation (19)) may be omitted from the calculation of the non-window absorptance $A_{c,nw}$. Since $p \gg e$ throughout the atmosphere, $A_{c,nw}$ is:

$$A_{c,nw} \simeq 1 - \int_{\nu_1}^{\nu_2} \exp\left[-k\left(\nu, \widetilde{T_p}\right) C_f(\nu) \int_{p_1}^{p_2} \frac{p}{p_0} dW(p)\right] d\nu \quad (22)$$

$$= 1 - \int_{\nu_1}^{\nu_2} \exp\left[-k\left(\nu, \widetilde{T_p}\right) C_f(\nu) U\right] d\nu \quad (23)$$

$$\simeq 1 - \int_{\nu_1}^{\nu_2} \exp\left[-k\left(\nu, \widetilde{T_p}\right) C_f(\nu) \widetilde{U_b}\right] d\nu \quad (24)$$

The last step (equation (24)) is valid because $U \simeq \widetilde{U_b}$ in the rotation and vibration-rotation bands. The wave number interval ν_1 to ν_2 is understood to lie in the non-window region. This calculation demonstrates that $A_{c,nw}$ may be approximated in terms of the scaling parameters for lines. Therefore Curtis-Godson scaling theory preserves the continuum absorption for inhomogeneous atmospheres outside the mid-IR window.

[19] Inside the window, the continuum absorptance is dominated by the self-component [*Clough et al.*, 1992]:

$$A_{c,w} \simeq 1 - \int_{\nu_1}^{\nu_2} \exp\left[-k\left(\nu, \widetilde{T_p}\right) C_s\left(\nu, T_{ref}\right) U_c(\nu)\right] d\nu \quad (25)$$

where $T_{ref} = 296K$ is a reference temperature, and the self-continuum path length is

$$U_c(\nu) = \int_{p_1}^{p_2} \frac{e}{p_0} \frac{C_s(\nu, T)}{C_s\left(\nu, T_{ref}\right)} dW(p) \quad (26)$$

The wave number interval ν_1 to ν_2 spans the midinfrared window. Since $C_s(\nu, T)$ is only weakly dependent on ν in

the mid-IR window, the self-continuum path length may be approximated by

$$U_c = \int_{p_1}^{p_2} \frac{q}{\epsilon} \frac{p}{p_0} \frac{C_s(\bar{\nu}, T)}{C_s\left(\bar{\nu}, T_{ref}\right)} dW(p) \tag{27}$$

where $\bar{\nu}$ is a suitably chosen wave number inside the window.

[20] In the equivalent homogeneous atmosphere defined by scaling theory, the value of the continuum path length is

$$\widetilde{U_c} = \frac{\widetilde{q}}{\epsilon} \frac{C_s\left(\bar{\nu}, \widetilde{T_p}\right)}{C_s\left(\bar{\nu}, T_{ref}\right)} U \tag{28}$$

Clearly U_c need not equal $\widetilde{U_c}$. In order to preserve the total absorption in the mid-IR window, it is necessary to define different equivalent homogeneous atmospheres for the lines and continuum. The parameters for the equivalent atmospheres differ only in the pressure-weighted path lengths. For the continuum, the pressure-weighted path length is calculated by setting $\widetilde{U_c} \rightarrow U_c$ and solving for $U' = U$:

$$U' = \frac{\epsilon}{\tilde{q}} \frac{C_s\left(\bar{\nu}, T_{ref}\right)}{C_s\left(\bar{\nu}, \widetilde{T_p}\right)} U_c \tag{29}$$

2.3.3. Total Line and Continuum Absorptance

[21] The analysis of the absorptance shows that the absorptivity and emissivity can be split into terms for the window and non-window portions of the infrared spectrum. The formalism is identical for the absorptivity and emissivity, and for brevity only the absorptivity is discussed in detail. The absorptivity is decomposed into two terms:

$$A(z, z') \simeq A_w(z, z') + A_{nw}(z, z') \tag{30}$$

where $A_w(z, z')$ is the window component and $A_{nw}(z, z')$ is the non-window component.

[22] The set of scaling parameters that determine the total non-window absorption are labeled:

$$l_{nw} = \left[\widetilde{U_{nw}}, \widetilde{P_{nw}}, T_e, \widetilde{T_p}, \tilde{\rho}\right] \tag{31}$$

The corresponding set of parameters for the line absorption in the window region are:

$$l_w = \left[\widetilde{U_w}, \widetilde{P_w}, T_e, \widetilde{T_p}, \tilde{\rho}\right] \tag{32}$$

The set of scaling parameters that determine the continuum absorption in the window are:

$$c_w = \left[U', \widetilde{P_w}, T_e, \widetilde{T_p}, \tilde{\rho}\right] \tag{33}$$

Table 3. Ranges of Independent Parameters in A and E

Parameter[a]	Units	Minimum	Maximum	Increment
$T_e - \widetilde{T_p}$	K	−120	80	10
$\widetilde{T_p}$	K	160	350	$21\frac{1}{9}$
$\log_{10}(\widetilde{P_b}/p_0)$	–	−3	0	$\frac{1}{3}$
$\log_{10}(\widetilde{U_b})$, $\log_{10}(U')$	log(g/cm^2)	−8	4	0.5
$\tilde{\rho}$	–	0	1.2	0.2

[a] p_0 = 1013.25 mbar.

Table 4. Calculation of Clear-Sky Surface Fluxes for H_2O Only[a]

Atmosphere	GENLN	CCM3.6 − GENLN	CAM − GENLN
High-Latitude Summer	111.5	−1.8	−2.1
High-Latitude Winter	111.4	12.4	1.5
Midlatitude Summer	94.9	−0.9	0.6
Midlatitude Winter	125.8	5.5	−0.6
Tropics	78.6	−2.8	−2.8
Mean Error	–	2.5 ± 6.4	−0.7 ± 1.8

[a] Fluxes are given in W/m^2.

[23] Let $\widetilde{A}_{nw}(i)$ represent the total non-window absorption for a homogeneous atmosphere characterized by a set of scaling parameters i. It follows from Curtis-Godson scaling theory that

$$A_{nw}(z, z') \simeq \widetilde{A}_{nw}(l_{nw}) \tag{34}$$

[24] The window term $A_w(z, z')$ requires a special provision for the different path parameters l_w and c_w for the lines and continuum. Let

$$\begin{aligned} \widetilde{A}_w(i) &= \text{absorptivity for scaling parameters } i, \text{ lines and continuum} \\ \widetilde{A}'_w(i) &= \text{absorptivity for scaling parameters } i, \text{ lines only} \end{aligned} \tag{35}$$

The lines-only absorptivity can be written in terms of a line transmission factor $L(i)$ and an asymptotic absorptivity A_∞ in the limit of a black-body atmosphere. A_∞ is a function only of T_e [*Ramanathan and Downey*, 1986]. The relationship is

$$\widetilde{A}'_w(i) = A_\infty[1 - L(i)] \tag{36}$$

Define an effective continuum transmission $C(i)$ by setting

$$\widetilde{A}_w(i) = A_\infty[1 - L(i)C(i)] \tag{37}$$

We approximate the window absorptivity by:

$$A_w(z, z') \simeq A_\infty[1 - L(l_w)C(c_w)] \tag{38}$$

This approximation for $A_w(z, z')$ can be cast entirely in terms of the absorptivities defined in equation (35). From equations (36) and (37), the line and continuum transmission are:

$$\begin{aligned} L(l_w) &= 1 - \frac{\widetilde{A}'_w(l_w)}{A_\infty} \\ C(c_w) &= \frac{A_\infty - \widetilde{A}_w(c_w)}{A_\infty - \widetilde{A}'_w(c_w)} \end{aligned} \tag{39}$$

Table 5. Calculation of Clear-Sky TOA Fluxes for H_2O Only[a]

Atmosphere	GENLN	CCM3.6 − GENLN	CAM − GENLN
High-Latitude Summer	300.0	4.3	1.0
High-Latitude Winter	222.6	1.9	−0.9
Midlatitude Summer	323.7	5.4	1.4
Midlatitude Winter	263.4	3.4	0.1
Tropics	333.1	5.8	2.3
Mean Error	–	4.2 ± 1.6	0.8 ± 1.2

[a] Fluxes are given in W/m^2.

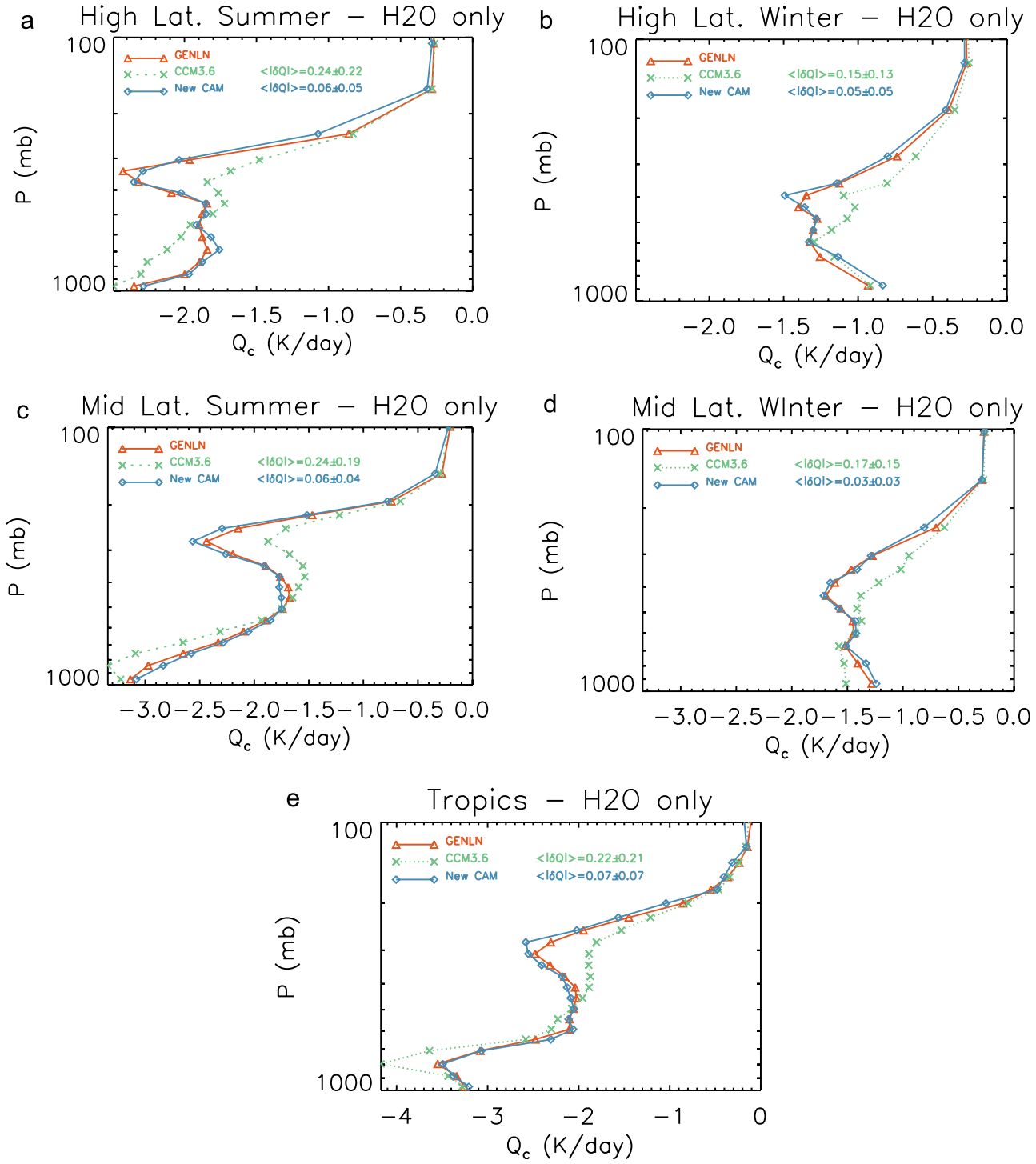

Figure 2. Clear-sky longwave cooling rates as a function of pressure between 100 and 1000 mbar. The rates are computed for the five standard AFGL atmospheres using GENLN (red), CCM3 (green), and the new CAM (blue). (a) High-latitude summer; (b) high-latitude winter; (c) midlatitude summer; (d) midlatitude winter; and (e) tropics. The values $\langle|\delta Q|\rangle$ give the mean and RMS differences relative to GENLN.

This completes the set of approximations used to calculate the absorptivity.

2.4. Calculation of Absorptivity and Emissivity

[25] As shown in section 2.3, the absorptivity $A(z, z')$ for an inhomogeneous atmosphere can be written in terms of the absorptivities $\widetilde{A}_{nw}(i)$, $\widetilde{A}_{w}(i)$, and $\widetilde{A}'_{w}(i)$ for equivalent homogeneous atmospheres (equations (34)–(39)). The decomposition of the emissivity follows the same formalism. The absorptivities and emissivities for equivalent atmospheres are computed by varying each independent path parameter (Table 2) over the range of values encoun-

Table 6. Components of Clear-Sky Surface Flux Differences for H_2O Only

Atmosphere	Total[a]	Rotation (L)	Rotation (C)	Vibration/ Rotation (L)	Vibration/ Rotation (C)	Window (L)	Window (C)
High-Latitude Summer	−1.8	4.6	−7.0	0.8	−0.9	2.5	−1.8
High-Latitude Winter	12.4	5.6	5.0	0.8	0.6	0.7	−0.3
Midlatitude Summer	−0.9	4.0	−5.8	0.9	−0.4	3.8	−3.4
Midlatitude Winter	5.5	5.3	−0.7	0.4	−0.2	1.2	−0.5
Tropics	−2.8	4.2	−4.7	0.7	−1.0	5.0	−7.0

[a] CCM3.6 – GENLN. The total differences are decomposed into the rotation, vibration/rotation, and window bands for lines (L) and the continuum (C). Fluxes are given in W/m^2.

tered in climate simulations. The range of values for each parameter has been determined using the instantaneous hourly fields from a multi-year integration of CAM. The probability distributions of each parameter (excluding pressure) are shown in Figure 1. The difference between emission and path temperatures is plotted to emphasize the large temperature gradients between the point of emission and the atmospheric path. The magnitude of these differences invalidates the use of isothermal absorptivities and emissivities [*Ramanathan and Downey*, 1986]. In the line-by-line calculation of the absorptivities and emissivities, the path parameters are varied across the entire range of atmospheric conditions shown in Figure 1. The minimum and maximum values and the increments within the range of each parameter are given in Table 3. Many of the resulting parameter combinations are unlikely to occur in practice but are included to handle unusual atmospheric conditions. Spectral transmissions for each parameter combination are generated with GENLN at 1 cm^{-1} resolution over the wave number range 0 to 2200 cm^{-1}. These are convolved with the Planck function or its derivative and integrated over the appropriate wave number intervals to compute the absorptivities and emissivities for homogeneous atmospheres.

3. Changes to Fluxes and Cooling Rates for Standard Atmospheres

3.1. Differences in Cooling Rates and Fluxes Relative to Line-By-Line Calculations

[26] The longwave surface fluxes, top-of-atmosphere (TOA) fluxes, and cooling rates computed with the updated scheme have been evaluated against GENLN calculations for the five standard AFGL atmospheres [*Anderson et al.*, 1986]. These calculations omit the effects of radiatively active trace gases in order to isolate the changes related to the treatment of water vapor. The upwelling flux at the surface and downwelling flux at TOA are prescribed. The differences in the surface fluxes between GENLN and the original and updated parameterizations are shown in Table 4, and the corresponding differences in the TOA fluxes are shown in Table 5. The sign convention is that net upwelling fluxes are positive. In general, the previous absorptivity/emissivity scheme overestimates the net upwelling fluxes at both the surface and TOA. In the updated scheme, the mean errors in the surface and TOA fluxes have been reduced to less than 1 W/m^2. Positive biases relative to GENLN indicate an underestimate of downwelling flux at the surface and an overestimate of upwelling flux at TOA.

[27] The largest biases in the surface fluxes calculated with the previous absorptivity/emissivity scheme occur in midlatitude and high-latitude winter. These calculations support the findings of *Lubin and Harper* [1996], *Pinto et al.* [1997], and *Briegleb and Bromwich* [1998], who show that the surface downwelling longwave flux from CCM is too large by 10–30 W/m^2 relative to observations in polar regions. The magnitude of the bias is less than 1.5 W/m^2 in the updated formulation. The TOA fluxes from the original method are larger than the corresponding fluxes from GENLN for all profiles. This indicates that the CCM consistently underestimates the water vapor greenhouse effect, which is the difference between the upwelling longwave fluxes at surface and TOA [*Raval and Ramanathan*, 1989; *Stephens and Greenwald*, 1991]. The errors in the method for calculating the greenhouse effect have been nearly eliminated in the updated approach. It should be noted that *Ramanathan and Downey* [1986] compared fluxes from the original absorptivity/emissivity scheme with LBL models and obtained much smaller differences than shown here. Unfortunately the LBL model results used in their original error analysis are not available, so it is not possible to isolate which elements of the updated LBL calculations are contributing to larger differences.

[28] The longwave cooling rates from the original and updated parameterizations and from GENLN are shown in Figure 2. The calculations and intercomparisons are sensitive to the assumed layering structure. If layering is too coarse, discontinuous gradients in state parameters can lead to apparent discontinuities in the heating rates. For all

Table 7. Components of Clear-Sky TOA Flux Differences for H_2O Only

Atmosphere	Total[a]	Rotation (L)	Rotation (C)	Vibration/ Rotation (L)	Vibration/ Rotation (C)	Window (L)	Window (C)
High-Latitude Summer	4.3	1.2	1.8	−0.1	0.6	1.2	−0.4
High-Latitude Winter	1.9	0.1	1.8	−0.4	0.2	0.3	−0.1
Midlatitude Summer	5.4	1.5	2.1	0.2	0.7	1.4	−0.5
Midlatitude Winter	3.4	0.7	2.1	−0.2	0.3	0.6	−0.1
Tropics	5.8	1.6	2.1	0.3	0.9	1.9	−1.0

[a] CCM3.6 – GENLN. The total differences are decomposed into the rotation, vibration/rotation, and window bands for lines (L) and the continuum (C). Fluxes are given in W/m^2.

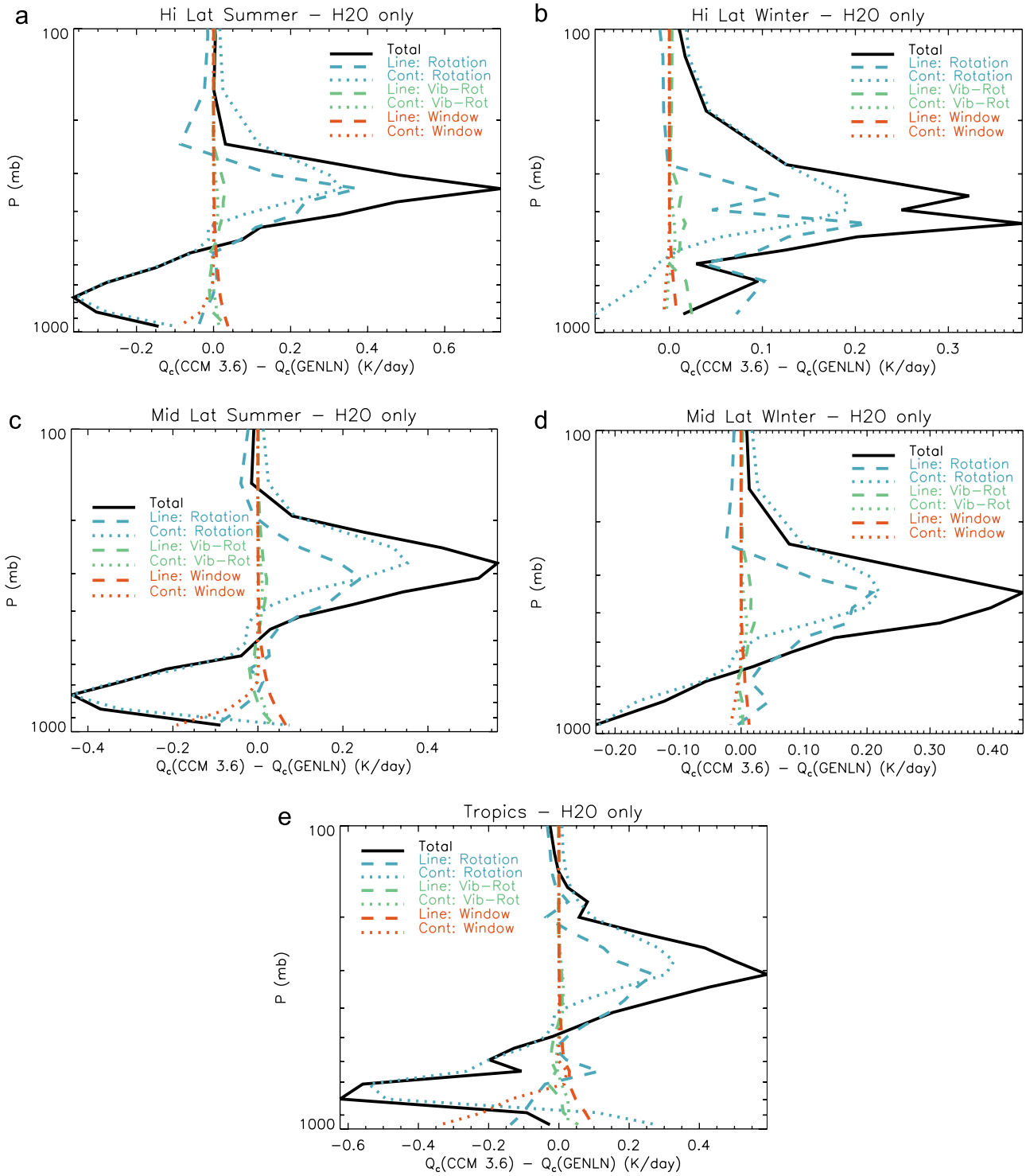

Figure 3. Differences in clear-sky longwave cooling rates as a function of pressure between 100 and 1000 mbar. The rates are computed for the five standard AFGL atmospheres using GENLN and CCM3 and then subtracted (CCM3.6 – GENLN). (a) High-latitude summer; (b) high-latitude winter; (c) midlatitude summer; (d) midlatitude winter; and (e) tropics.

profiles except high-latitude winter, the differences between rates computed from GENLN and the original parameterization exhibit a dipole profile. The original parameterization underestimates the longwave cooling near 300 mbar by 0.4 to 0.7 K/d, and it overestimates the cooling rate near 800 mbar by 0.2 to 0.6 K/d. The biases in the cooling rates near 300 mbar are noted in the description of the original absorptivity/emissivity formulation [*Ramanathan and Downey*, 1986]. For high-latitude winter, the original method underestimates the cooling rate at all

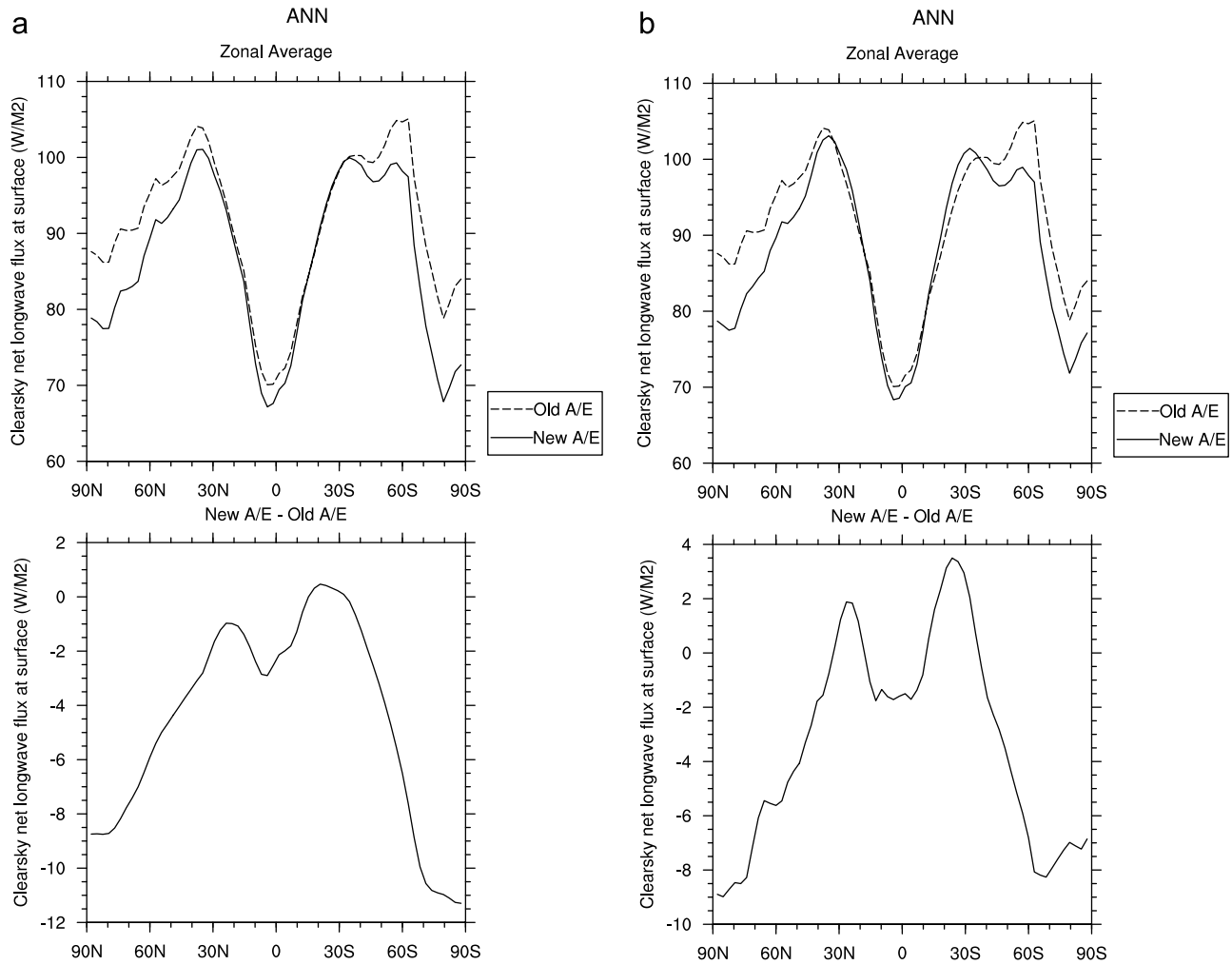

Figure 4. Zonally and annually averaged surface clear-sky longwave fluxes from CAM. (a) Zonal-mean values and differences of $F_{c,i}^{old}(0)$ and $F_{c,d}^{new}(0)$ from integration I^{old}; and (b) zonal-mean values and differences of $F_{c,i}^{old}(0)$ and $F_{c,i}^{new}(0)$ from integrations I^{old} and I^{new}, respectively.

pressures between 100 and 1000 mbar. In the stratosphere (not shown), the errors between the original formulation and GENLN are typically less than 0.02 K/d. The accuracy of the updated treatment is comparable, with differences relative to GENLN of 0.05 K/d or less. Both the original and new schemes slightly overestimate the cooling in the stratosphere due to H_2O when compared to the line-by-line calculations.

[29] The updated parameterization reduces the mean and RMS differences relative to GENLN in each profile by at least a factor of 3. In addition, the dipole pattern is not evident in the errors in cooling rates from the updated approach. Since the tendency in atmospheric temperature depends upon the longwave cooling rates, the significant differences in δQ between the original and updated parameterizations should affect the mean climate state simulated by the model. The changes in the mean climate are examined in section 5.

3.2. Analysis of Differences by Spectral Band

[30] The biases in the original formulation for CCM can be decomposed into errors associated with line and continuum absorption in the rotation, window, and vibration-rotation bands. Consistent definitions of continuum and line absorption have been used throughout. The portion of the line absorption that CKD includes in its definition of the continuum is subtracted from the total line absorption. The fluxes and cooling rates for the three bands are computed with GENLN for lines only and for lines and continuum. The effects of the continuum are isolated by subtracting the calculation for lines alone from the calculation with lines and continuum. The decomposition for the surface and TOA fluxes are shown in Tables 6 and 7, respectively. Note that the continuum is not included in the original parameterization for $\nu < 500$ cm^{-1}, and this omission will increase the differences in the rotation-band continuum terms. It is also omitted for $\nu > 1200$ cm^{-1}, i.e. over the entire vibration/rotation band. With the exception of the tropical surface flux, the main terms in the total biases are contributed by the rotation band. At the surface, the biases in the line terms are offset by biases in the continuum terms of opposite sign for each band. The one profile which differs from this pattern is high-latitude winter. At TOA, the biases in the rotation band are additive,

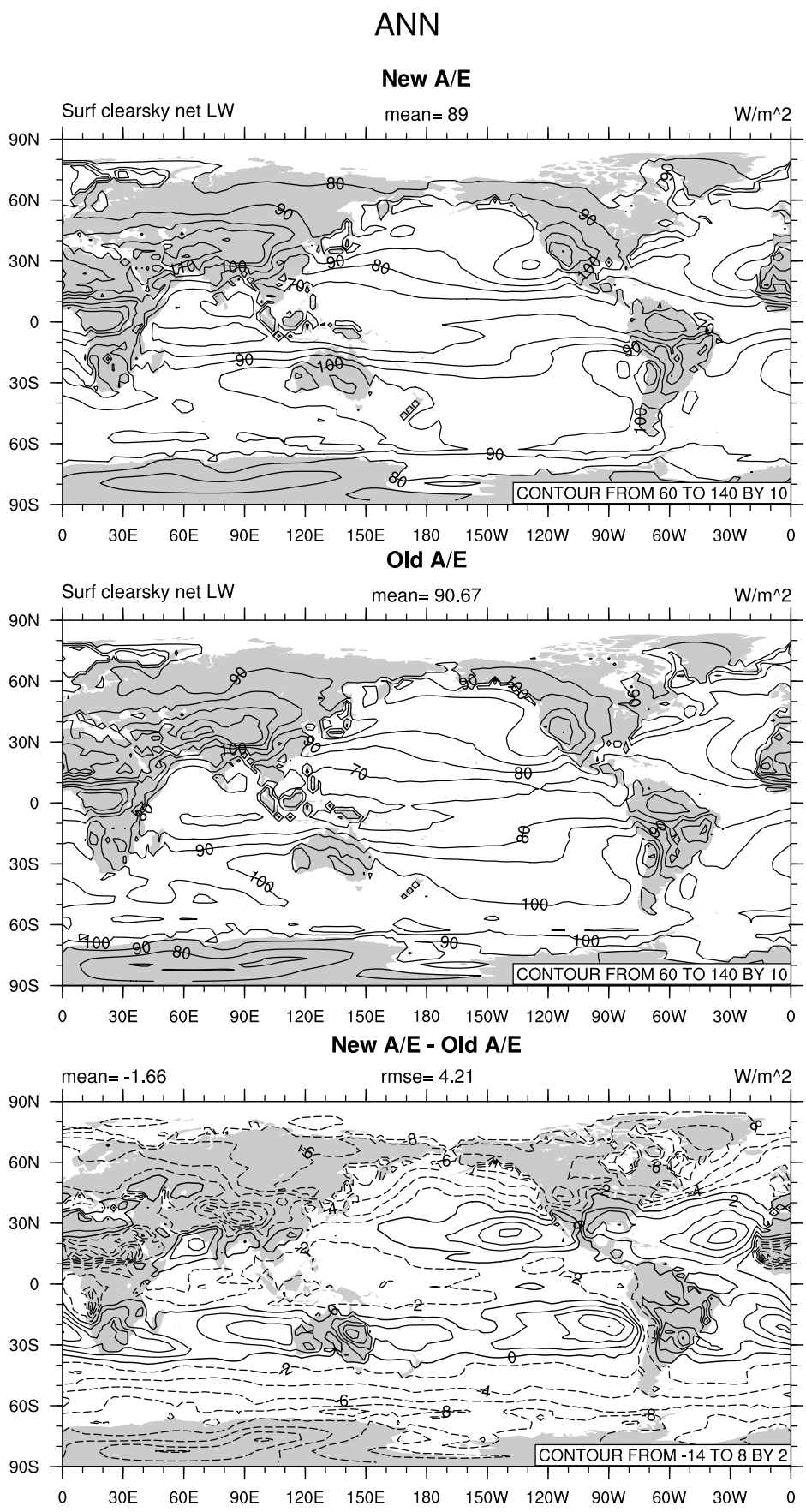

Figure 5. Annually averaged surface clear-sky longwave fluxes from CAM. (top) $F_{c,i}^{new}$ from integrations I^{new}; middle panel: $F_{c,i}^{old}$ from integration I^{old}; and (bottom) $F_{c,i}^{new} - F_{c,i}^{old}$.

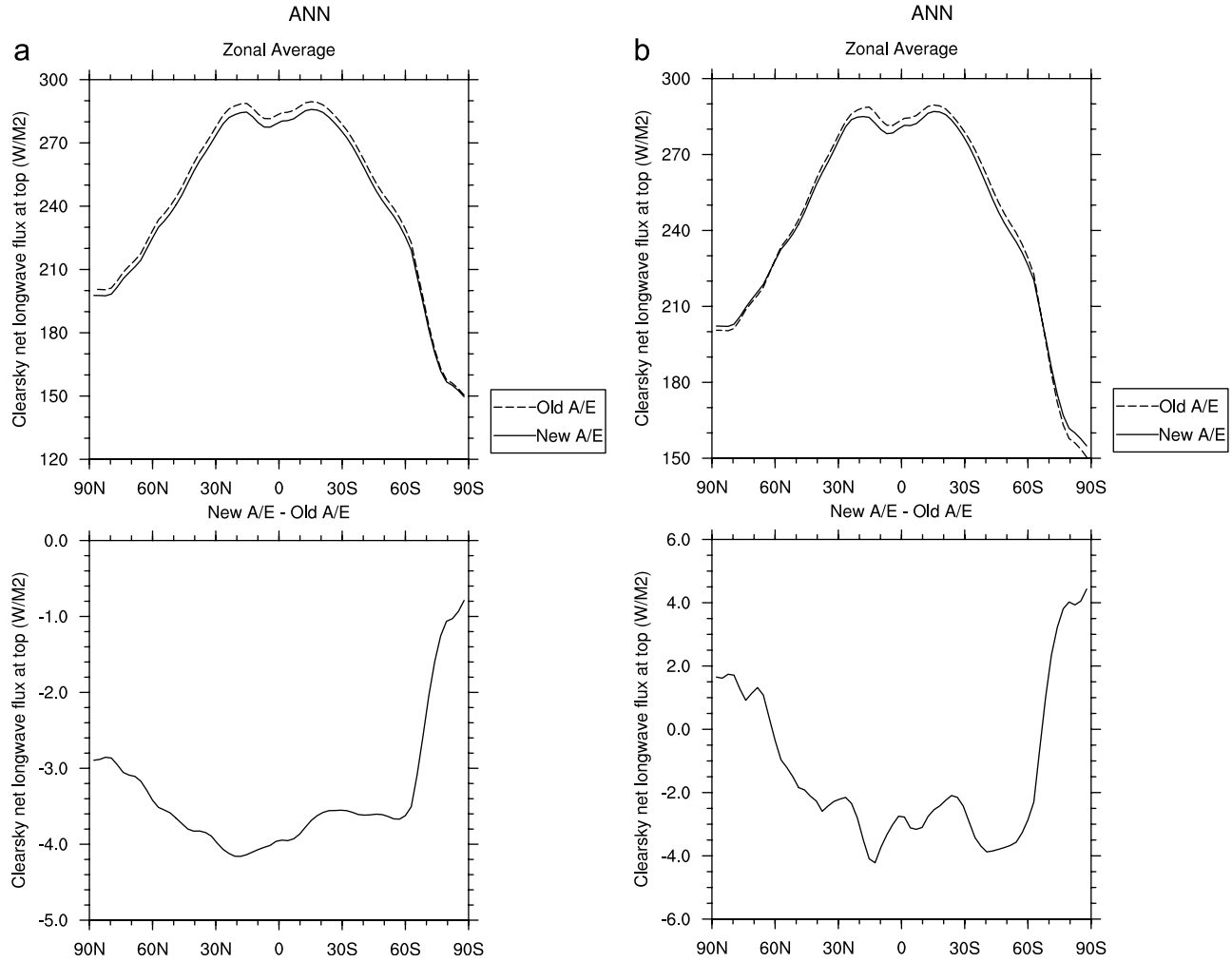

Figure 6. Zonally and annually averaged TOA clear-sky longwave fluxes from CAM. (a) Zonal-mean values and difference of $F_{c,i}^{old}(TOA)$ and $F_{c,d}^{new}(TOA)$ from integration I^{old}; and (b) zonal-mean values and differences of $F_{c,i}^{old}(TOA)$ and $F_{c,i}^{new}(TOA)$ from integrations I^{old} and I^{new}, respectively.

although there is still some cancellation between the line and continuum errors in the window.

[31] The differences in cooling rates calculated from the original method and GENLN in each band are plotted in Figure 3. The differences are dominated by biases in the rotation band. The underestimate of cooling near 300 mbar results from nearly equal errors in the cooling contributed by line and continuum absorption in the rotation band. The bias in the continuum cooling results from differences in the formulation of the foreign continuum and the omission of continuum absorption between 0 and 500 cm^{-1} in the original method. With the exception of high-latitude winter, the overestimate of cooling near 800 mbar is almost entirely due to the formulation of the self-continuum in the rotation band. For relatively moist conditions in the summer hemisphere and in the tropics, the second largest error near the surface is contributed by the self-continuum in the window. Errors in the cooling by the rotation/vibration and window bands are less than 0.05 K/d between 100 mbar and 700 mbar for all five standard atmospheres. This analysis demonstrates that the differences in cooling rates are caused primarily by differences between the Roberts and CKD continuum and between the estimates of line absorption in the rotation band.

4. Changes to Fluxes and Cooling Rates in the Community Atmosphere Model

[32] The response of the model to the changes in the longwave effects of H_2O have been evaluated with two integrations of CAM. In the first, the original scheme is run interactively with the rest of the model, and the updated scheme is run diagnostically against the same atmospheric states. Both sets of fluxes and cooling rates are archived. In the second integration, the updated scheme is interactive and the original scheme is diagnostic. The simulations are labeled I^{old} and I^{new}, respectively. Both integrations have been run for 6 years, and the last 5 years are averaged for comparison against each other and against observations. The sea-surface temperatures are taken from an annually cyclic climatology of monthly mean satellite retrievals. The land-surface conditions are computed using the NCAR Common Land Model. Let $F_{c,k}^{j}(0)$ and $F_{c,k}^{j}(TOA)$ represent the clear-sky fluxes at the surface and TOA for absorptivity/

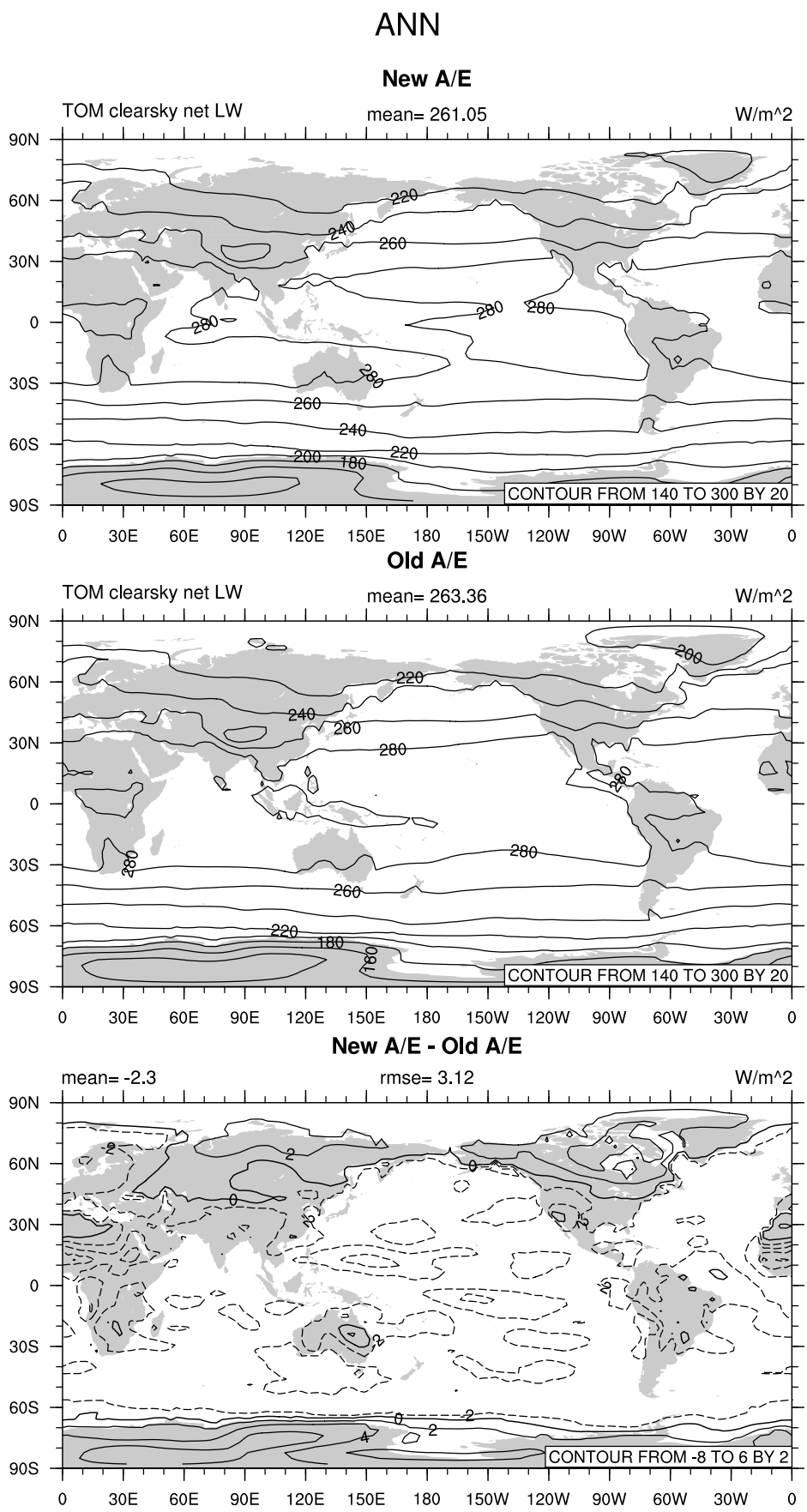

Figure 7. Annually averaged TOA clear-sky longwave fluxes from CAM. (top) $F_{c,i}^{new}(TOA)$ from integrations I^{new}; (middle) $F_{c,i}^{old}(TOA)$ from integration I^{old}; and (bottom) $F_{c,i}^{new}(TOA) - F_{c,i}^{old}(TOA)$.

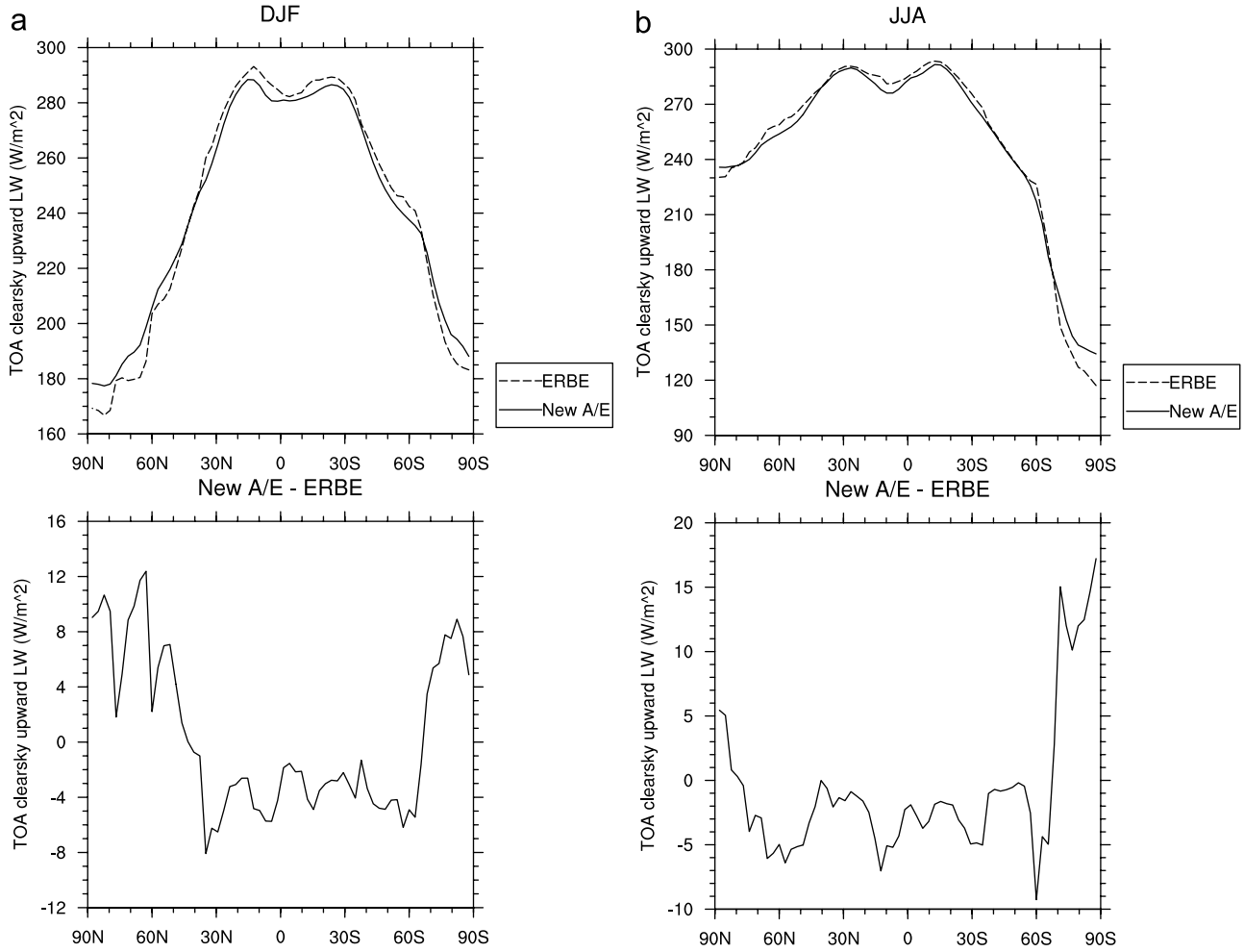

Figure 8. Zonally and seasonally averaged clear-sky outgoing longwave radiation from the new radiation scheme and the 5-year ERBE data set. (a) Average fluxes and flux difference for December through February; (b) Average fluxes and flux difference for June through August.

emissivity scheme j and integration k. Let $j = old$ and $j = new$ denote the original and updated methods and $k = d$ and $k = i$ denote the diagnostic or interactive status of the flux calculation. The corresponding clear-sky and all-sky cooling rates are $Q^j_{c,k}$ and Q^j_k. Departures of the modeled fluxes from corresponding fields in meteorological analyses and radiation data sets reflect differences both in radiative transfer methods and the input thermodynamic profiles. The optimum test of the accuracy of the updated absorptivity/emissivity method is comparison against benchmark LBL codes as discussed in section 3. Some of the differences between the integrations with the original and updated schemes reflect feedbacks on the simulated climate state from the changes in the longwave diabatic cooling rates. These feedbacks are examined in section 5.

[33] The zonally and annually averaged clear-sky surface fluxes are shown in Figure 4. For comparison, fluxes from the updated scheme run in a diagnostic and interactive mode are compared against fluxes from the previous parameterization run in interactive mode. In the diagnostic comparison, the zonal-mean flux $F^{new}_{c,d}(0)$ is less than $F^{old}_{c,i}(0)$ at almost all latitudes. The largest differences occur in the polar regions of both hemispheres with a secondary local maximum centered on the equator. The reduction in net flux near the poles occurs during both summer and winter seasons (not shown). The difference $F^{new}_{c,i}(0) - F^{old}_{c,i}(0)$ when both fluxes are computed interactively displays a similar meridional pattern, although the differences are shifted toward positive values everywhere except 63S to 42S and 85N to 90N. The change from the original to updated method changes the net clear-sky flux by 2 to 3.5 W/m^2 at latitudes corresponding to the descending branches of the Hadley circulation. The largest local increases in the interactive calculation occur in the eastern regions of the Atlantic, Pacific, and Indian oceans at approximately 30N and 30S (Figure 5). The largest local decreases for continental regions at low latitudes occur over central Africa and the Tibetan Plateau.

[34] The zonally and annually averaged clear-sky TOA fluxes are shown in Figure 6. The flux $F^{old}_{c,i}(TOA)$ computed with the original absorptivity/emissivity scheme is compared against fluxes $F^{new}_{c,d}(TOA)$ and $F^{new}_{c,i}(TOA)$ computed with the updated scheme run in diagnostic and interactive modes. In the diagnostic calculation, the TOA flux decreases at all latitudes. Therefore, in the absence of feedbacks on the climate state, the updated scheme

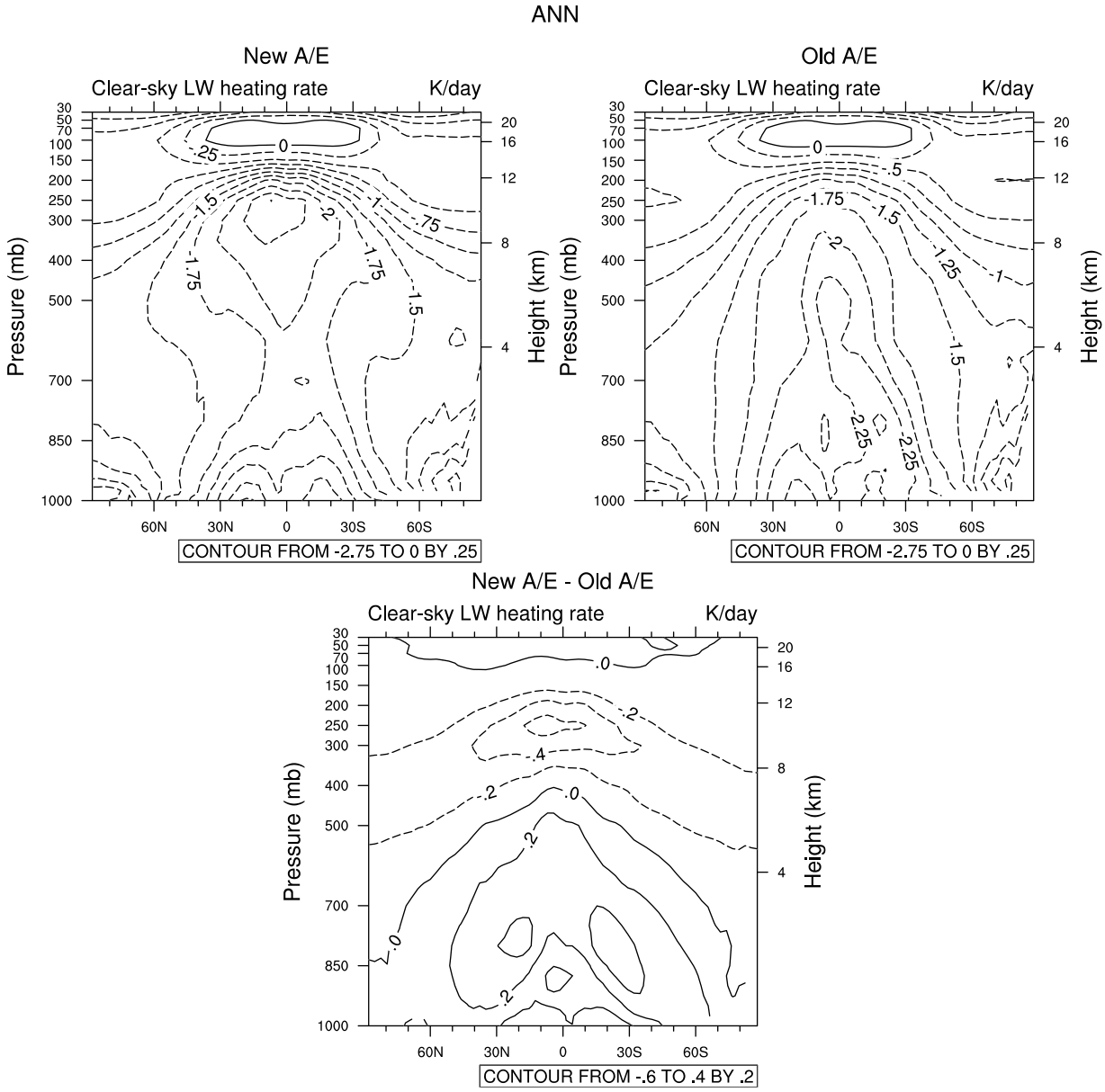

Figure 9. Zonally and annually averaged clear-sky longwave cooling rates from CAM. (top left) $Q_{c,i}^{new}$ from integration I^{new}; (top right) $Q_{c,i}^{old}$ from integration I^{old}; and (bottom) $Q_{c,i}^{new} - Q_{c,i}^{old}$.

increases the zonal-mean greenhouse effect of water vapor. The largest increase in the greenhouse effect, between 3.5 and 4 W/m^2, occurs in the tropics and subtropics. In the comparison with both schemes running interactively, the difference between the updated and original clear-sky net fluxes is positive in polar and subpolar regions in both hemispheres. However, the zonal-mean $F_{c,i}^{new}(TOA)$ is still smaller than $F_{c,i}^{old}(TOA)$ at all latitudes between 68S and 62N. Maps of the fluxes (Figure 7) show the zonal nature of the changes in TOA flux. In the tropics, the largest decreases occur over central Africa. In the Pacific, the TOA flux decreases by more than 6 W/m^2 in the western Pacific warm pool and the Southern Tropical Convergence Zone. The largest increases occur over Canada in the northern hemisphere and Antarctica in the southern hemisphere.

[35] The seasonally averaged clear-sky outgoing longwave fluxes from the updated scheme and from the Earth Radiation Budget Experiment (ERBE) are compared in Figure 8. Five-year means have been computed from the ERBE data set, which extends from December 1984 through February 1990 [*Harrison et al.*, 1990]. During December through February (DJF), the model underestimates the global-mean clear-sky OLR by 1.8 W/m^2 relative to ERBE. During June through August (JJA), the model underestimates the clear-sky OLR by 2.4 W/m^2. In both DJF and JJA, the model value of $F_{c,i}^{new}$ is lower than observed in the tropics between 30S to 30N. The biases in DJF and JJA relative to ERBE are -3.6 W/m^2 and -3.1 W/m^2, respectively. In CCM, the offsets relative to ERBE in the tropics are positive [*Kiehl et al.*, 1998b], so the updated parameterization reverses the sign of the systematic errors.

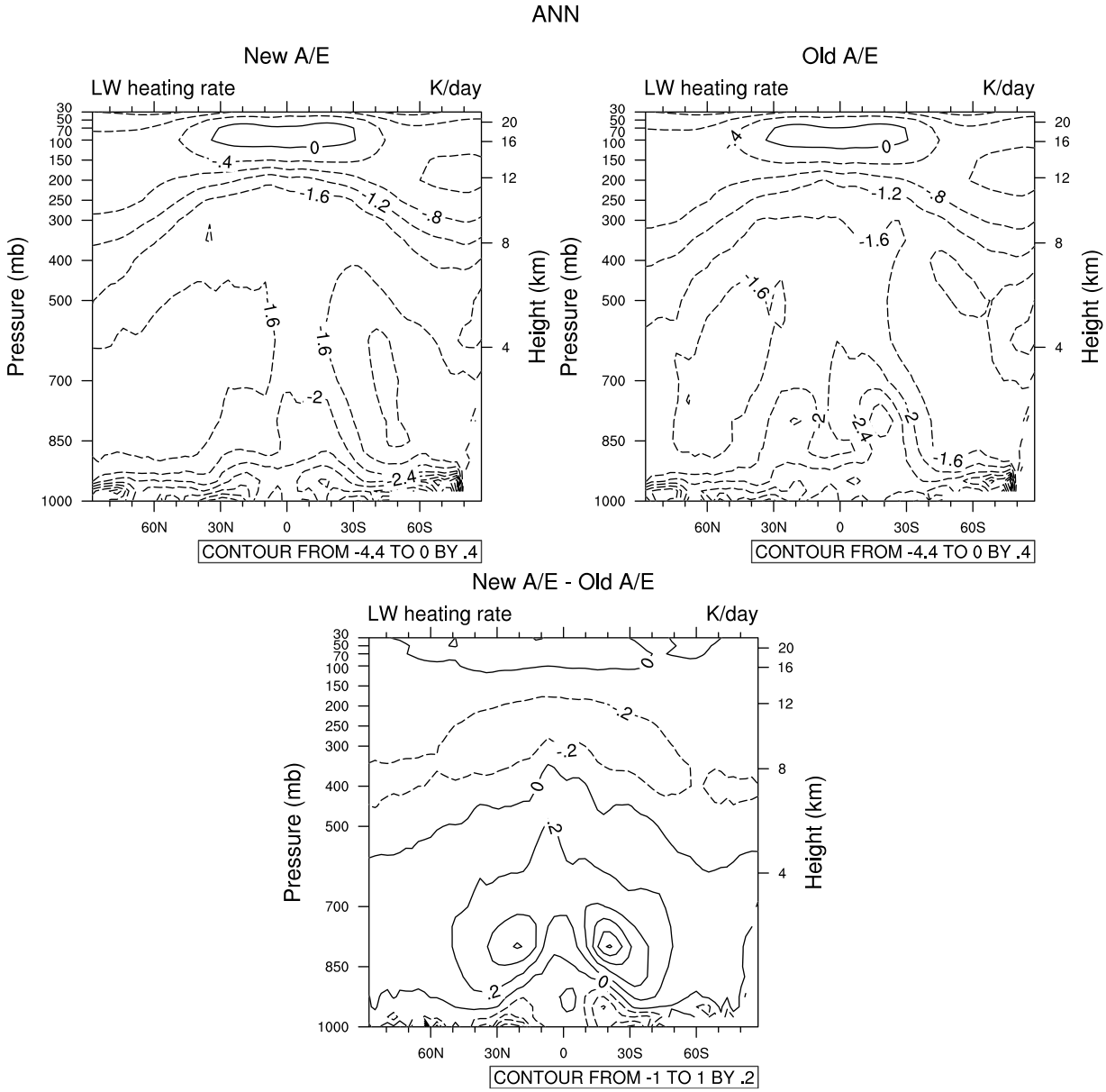

Figure 10. Zonally and annually averaged all-sky longwave cooling rates from CAM. (top left) Q_i^{new} from integration I^{new}; (top right) Q_i^{old} from integration I^{old}; and (bottom) $Q_i^{new} - Q_i^{old}$.

During both seasons, the negative offsets in the tropics are partially offset by larger positive biases in polar regions, especially in the winter hemisphere. Based upon the interannual internally forced variability in CAM, the differences between the modeled and observed clear-sky OLR are statistically significant. Part of the differences between CAM and ERBE may be attributable to biases in ERBE related to cloud screening techniques [*Collins and Inamdar*, 1995].

[36] The zonally and annually averaged difference $Q_{c,i}^{new} - Q_{c,i}^{old}$ in the clear-sky cooling rates between the updated and original parameterizations is plotted in Figure 9. The changes in the cooling rates from the CAM exhibit the same vertical profile observed in the offline calculations (Figure 2). At all latitudes, the cooling in the middle and upper troposphere is larger. The cooling increases by more than 0.5 K/d between 225 and 270 mbar between 18S to 26N. The cooling decreases in the planetary boundary layer and the lowest layers in the free troposphere. The largest reductions in cooling, which exceed 0.5 K/d, occur between 26S and 15S at approximately 790 mbar. The corresponding difference Q_i^{new} ndash; Q_i^{old} in the all-sky cooling rates is shown in Figure 10. In the free troposphere, the all-sky differences also have a dipole structure in the vertical direction. The magnitude of the change in cooling rate in the upper troposphere is roughly 60% of the change under clear-sky conditions. Note that the all-sky cooling increases near the surface at all latitudes in the interactive calculation. This increased cooling is not present in the diagnostic calculation for Q_d^{new}, and it therefore is a result of feedbacks between the updated longwave parameterization and the simulated climate state. The differences between the clear-

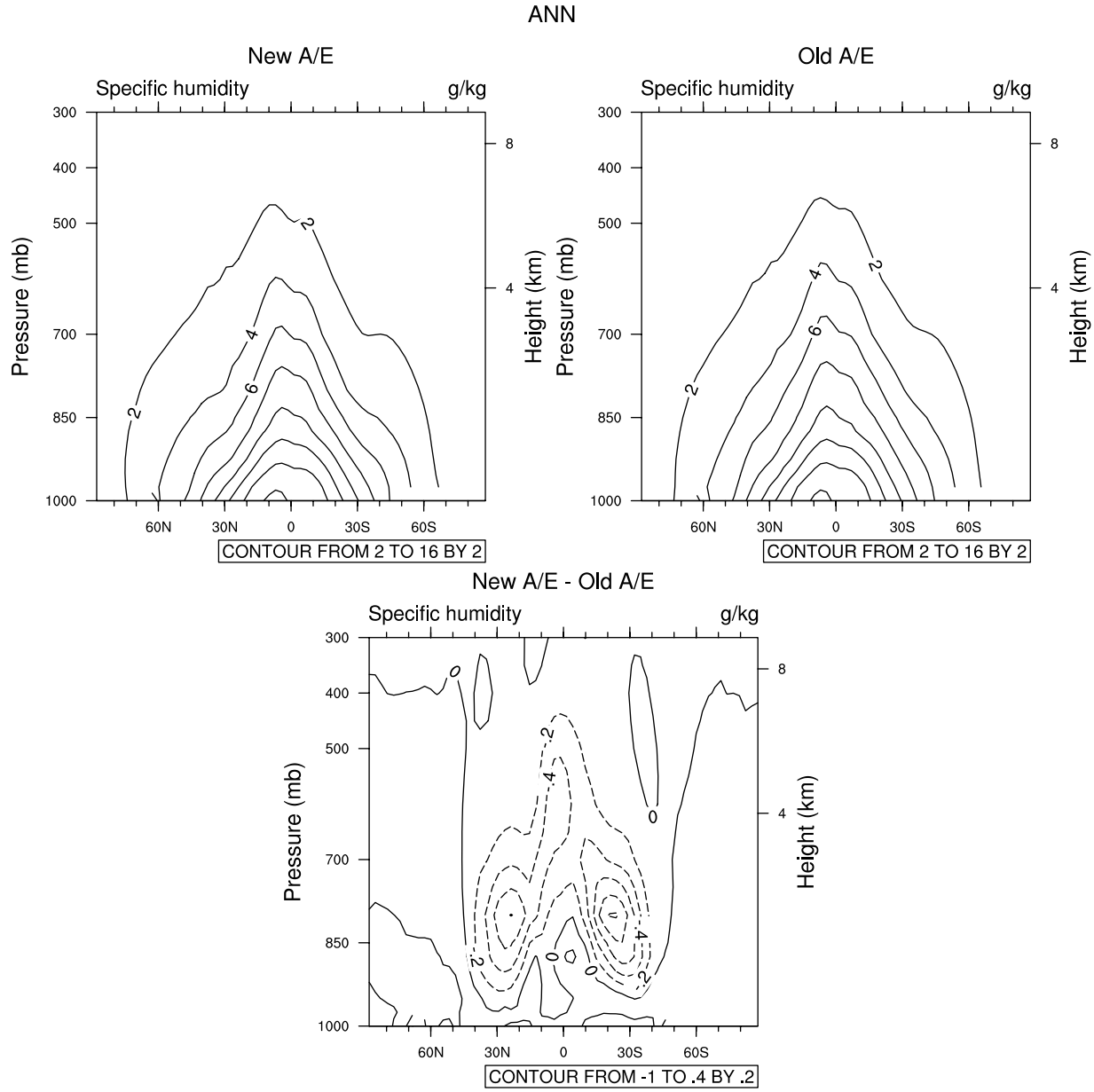

Figure 11. Zonally and annually averaged specific humidity q from CAM. (top left) q from integration I^{new}; (top right) q from integration I^{old}; and (bottom) difference in q (integration I^{new} minus I^{old}).

sky and all-sky heating rates are statistically significant at the 95% confidence level over 77% and 70% of the model domain between 30 mbar and the surface, respectively. These statistics are computed from the relatively short integrations used to construct Figures 9 and 10 and should only approximate the true significance values.

5. Discussion of Climate Feedbacks Related to Water Vapor Cooling Rate

[37] When the updated scheme is introduced into CAM, the simulated thermodynamic state of the atmosphere changes considerably. The large response is not surprising given the substantial changes in the longwave diabatic heating rates introduced by the updated scheme. One of the largest changes is related to the amount and distribution of moisture in the atmosphere. The differences in the specific humidity q are plotted in Figure 11. The specific humidity is reduced by at least 0.3 g/kg in the lower and middle troposphere between 30S and 30N. A qualitatively similar drying of the tropical atmosphere with a similar spatial distribution occurs when the longwave parameterization is replaced with a correlated-k radiative transfer code [*Iacono et al.*, 2000].

[38] The drying of the tropical atmosphere is one disadvantageous side-effect of improving the representation of longwave radiative transfer. In its standard configuration, the CCM simulates 15–20% less precipitable water than observed in the southern Indian Ocean, South Pacific convergence zone, equatorial Atlantic, and northern Africa [*Hack et al.*, 1998]. Additional drying would further degrade the fidelity of the mean seasonal and annual-mean

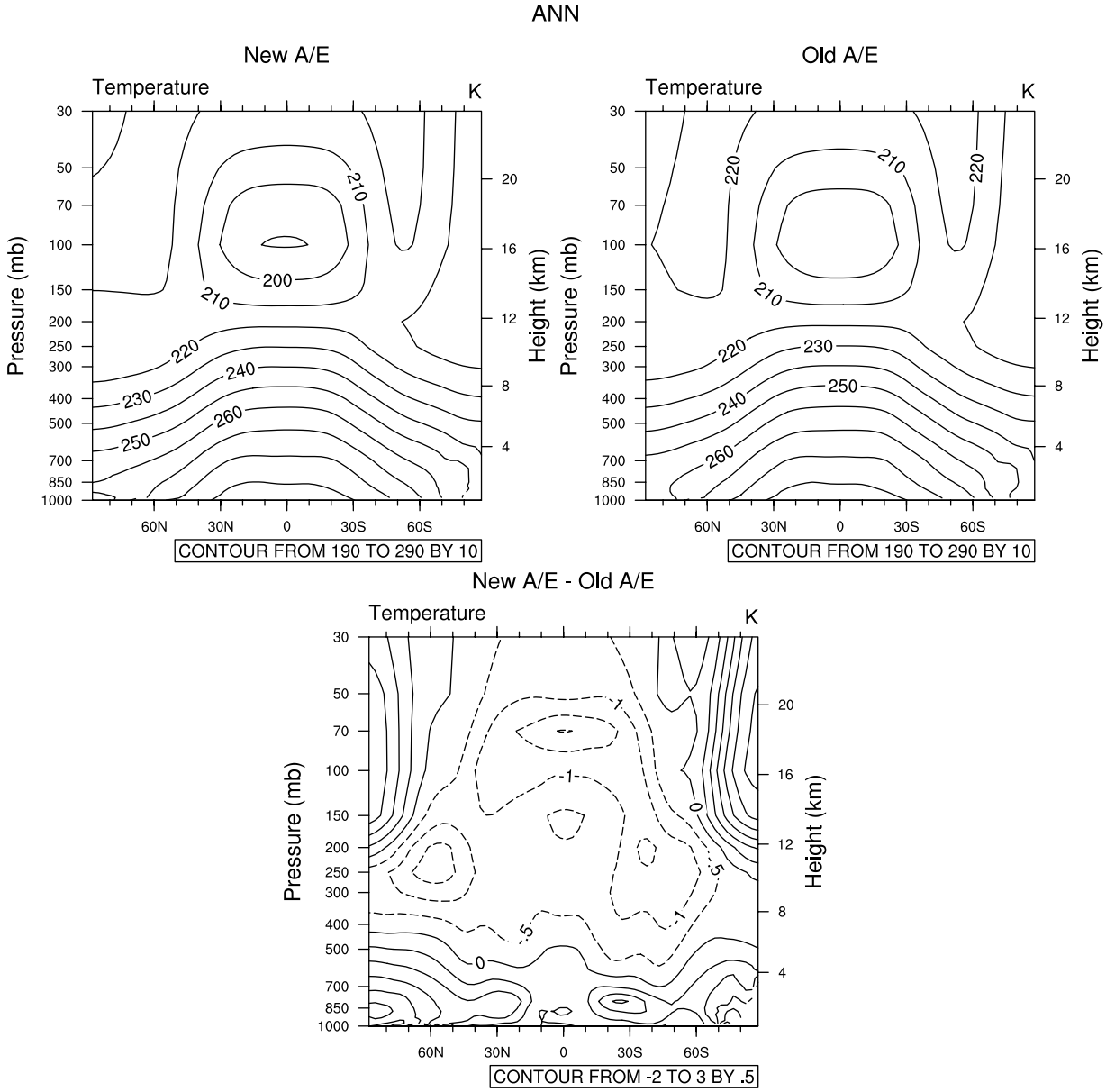

Figure 12. Zonally and annually averaged atmospheric temperature T from CAM. (top left) T from integration I^{new}; (top right) T from integration I^{old}; and (bottom) difference in T (integration I^{new} minus I^{old}).

climate state compared with meteorological analyses, soundings, and satellite retrievals. In order to counteract the effects of the updated longwave scheme on the precipitable water, the CAM includes evaporation of precipitation from convective anvil clouds following *Sundqvist* [1988]. The evaporation of precipitation is a significant source of moisture in regions of the tropics most strongly affected by the updated longwave parameterization. The integrations I^{old} and I^{new} discussed here include the evaporation term in the prognostic equation for q. As a result, the change in q from changing longwave schemes (Figure 11) is considerably smaller than observed in earlier prototypes of CAM or in the simulations by *Iacono et al.* [2000].

[39] One other consequence of the updated parameterization is a reduction in atmospheric temperature over most of the middle and upper tropical troposphere (Figure 12). The peak reduction of 2 K occurs near 70 mbar in the lower stratosphere. At 100 mbar, the changes range from an increase of 3.5 K at the South Pole to a decrease of 1 K to 1.5 K between 30S to 30N. The changes in polar regions help offset large negative biases in the temperatures simulated by CCM [*Hack et al.*, 1998]. However, the decrease in temperatures near the tropical tropopause exacerbates existing systematic errors relative to NCEP meteorological analyses. Reduction of these errors is critical for simulating the moisture flux into the stratosphere, and future development of CAM will include efforts to reduce the cold temperature bias. The differences between the specific humidities and temperatures rates are statistically significant at the 95% confidence level over 69% and 77% of the

model domain between 30 mbar and the surface, respectively. As in the case of the statistical analysis of the heating-rate differences, these values should be considered approximate given the five-year duration of the model integrations.

6. Conclusions

[40] An updated parameterization of the absorption and emission of longwave radiation by water vapor has been developed for the NCAR CAM, the successor to the Community Climate Model (CCM). The parameterization retains the formulation of the longwave radiative transfer equations in terms of absorptivity and emissivity. The updated scheme should be viewed as an interim solution for improving the accuracy of the radiation code relative to line-by-line models while the developers continue examining and testing correlated-k codes.

[41] The updated absorptivity and emissivity tables are computed using the GENLN2 LBL code. The data on H_2O line parameters is from the HITRAN-96 data base, and the continuum is treated using the CKD continuum version 2.1. In the previous approach, the line absorption has been fit to the Malkmus band model in the strong-line limit neglecting the effects of self-line-broadening. The continuum has been treated following *Roberts et al.* [1976] in the wave number range 500–1200 cm^{-1}. The updated approach includes the effects of self-broadening without parametric fitting to the Malkmus model. The self- and foreign-broadened continuum is treated following *Clough et al.* [1989] for the wave number range 0–2200 cm^{-1}.

[42] Errors in fluxes and heating rates computed for standard atmospheres are substantially reduced with the updated parameterization. The calculations omit other radiatively active gases in order to isolate the effects of the revised H_2O absorptivity and emissivity. The mean errors in cooling rates between 100 and 1000 mbar are less than 0.1 K/d for all atmospheres. The updated method eliminates a dipole bias in cooling rates calculated with the previous scheme. Decomposition by spectral band shows that the previous scheme underestimates cooling near 300 mbar by lines and the foreign continuum in the rotation band, and it overestimates cooling near 800 mbar by the self-continuum in the rotation band. The magnitude of mean errors in surface and TOA clear-sky fluxes are reduced to less than 1 W/m^2. The updated method increases the downwelling flux in polar regions by approximately 10 W/m^2. This change improves the fidelity of the surface clear-sky longwave fluxes in the Arctic and Antarctic when compared against surface observations.

[43] When the updated parameterization is introduced into the CAM, the changes in clear-sky longwave fluxes and cooling rates are qualitatively similar to the changes found in offline calculations. There is, however, a substantial change in the mean climate state driven by the interaction of the updated longwave diabatic heating rates and the parameterization for deep convection. The most substantial changes are a reduction in precipitable water in the tropics and subtropics and a reduction in tropopause temperature. The change in precipitable water is directly related to the response of the deep convective parameterization in CAM to the updated vertical profile of longwave cooling.

[44] Future work will address the effects of the updated longwave parameterization on the climate sensitivity of the model. This is particularly important since water feedbacks amplify the radiative effects of doubling carbon dioxide considerably [*Ramanathan*, 1981]. The updated scheme brings CAM into good agreement with modern LBL codes. Comparison of the original and updated parameterizations highlights the importance of physics in the far infrared for the simulated climate state. Almost all the changes in the longwave cooling rate for the upper troposphere are in the rotation band, a region of the spectrum that has not been intensively studied with field observations. Approximately half the change in the cooling rate is associated with the foreign continuum in the rotation band. Although recent field campaigns have begun to address the substantial uncertainties in the strength and temperature dependence of the foreign continuum [e.g., *Tobin et al.*, 1999], it is critical that further intensive studies be conducted. Modern climate models are converging to a single representation of continuum absorption, and experimental verification of the continuum under many atmospheric conditions is an important test of this model physics.

[45] **Acknowledgments.** The authors would like to acknowledge several helpful discussions with L. Donner (GFDL), J. J. Hack (NCAR), J. T. Kiehl (NCAR), V. Ramanathan (SIO/UCSD), V. Ramaswamy (GFDL), and A. Vogelmann (SIO/UCSD). M. Iacono (AER), D. Kratz (NASA Langley), and D. Schwarzkopf (GFDL) generously provided results from their radiative transfer models for evaluation of our updated parameterization. E. Kluzek and J. Truesdale (NCAR) helped implement and test the updated scheme, and M. Stevens (NCAR) assisted in evaluating the effects of the updated scheme in the full climate model. G. Francis (NCAR) advised us on how to modify and use the line-by-line code GENLN2. Comments by an anonymous reviewer helped the authors make significant improvements in the manuscript. This research was supported by the NOAA-NASA Climate and Global Change grant NA96GP0444 (WDC and JKH) and by NASA UARS Special Investigator grant S-10110-X (DPE). The National Center for Atmospheric Research is sponsored by the National Science Foundation.

References

Anderson, G. P., S. A. Clough, F. X. Kneizys, J. H. Chetwynd, and E. P. Shettle, AFGL atmospheric constituent profiles (0–120 km), *Tech. Rep. AFGL-TR-86-0110*, Air Force Geophys. Lab., Hanscom Air Force Base, Mass., 1986.

Briegleb, B. P., and D. H. Bromwich, Polar radiation budgets of the NCAR CCM3, *J. Clim.*, *11*, 1246–1286, 1998.

Clough, S. A., F. X. Kneizys, and R. W. Davies, Line shape and the water vapor continuum, *Atmos. Res.*, *23*, 229–241, 1989.

Clough, S. A., M. J. Iacono, and J. L. Moncet, Line-by-line calculations of atmospheric fluxes and cooling rates: Application to water vapor, *J. Geophys. Res.*, *97*, 15,761–15,785, 1992.

Collins, W. D., Parameterization of generalized cloud overlap for radiative calculations in general circulation models, *J. Atmos. Sci.*, *58*, 3224–3242, 2001.

Collins, W. D., and A. K. Inamdar, Validation of clear-sky fluxes for tropical oceans from the Earth Radiation Budget Experiment, *J. Clim.*, *8*, 569–578, 1995.

Curtis, A. R., Contribution to a discussion of "A statistical model for water vapour absorption" by R. M. Goody, *Q. J. R. Meteorol. Soc.*, *78*, 638–640, 1952.

Edwards, D. P., GENLN2: A general line-by-line atmospheric transmittance and radiance model, *Tech. Rep. NCAR/TN-367+STR*, 147 pp., Natl. Cent. for Atmos. Res., Boulder, Colo., Jan. 1992.

Godson, W. L., The evaluation of infra-red radiative fluxes due to atmospheric water vapour, *Q. J. R. Meteorol. Soc.*, *79*, 367–379, 1953.

Goody, R. M., and Y. L. Yung, *Atmospheric Radiation*, 2nd ed., 519 pp., Oxford Univ. Press, New York, 1989.

Hack, J. J., J. T. Kiehl, and J. W. Hurrell, The hydrologic and thermodynamic characteristics of the NCAR CCM3, *J. Clim.*, *11*, 1179–1206, 1998.

Han, Y., J. A. Shaw, J. H. Churnside, P. D. Brown, and S. A. Clough, Infrared spectral radiance measurements in the tropical Pacific atmosphere, *J. Geophys. Res.*, *102*, 4353–4356, 1997.

Harrison, E. F., P. Minnis, B. R. Barkstrom, V. Ramanathan, R. D. Cess, and G. G. Gibson, Seasonal variation of cloud radiative forcing derived from the Earth Radiation Budget Experiment, *J. Geophys. Res.*, *95*, 18,687–18,703, 1990.

Iacono, M. J., E. J. Mlawer, S. A. Clough, and J. J. Morcrette, Impact of an improved longwave radiation model, RRTM, on the energy budget and thermodynamic properties of the NCAR Community Climate Model, CCM3, *J. Geophys. Res.*, *105*, 14,873–14,890, 2000.

Kiehl, J. T., and K. E. Trenberth, Earth's annual global mean energy budget, *Bull. Am. Meteorol. Soc.*, *78*, 197–208, 1997.

Kiehl, J. T., J. Hack, G. Bonan, B. Boville, B. Briegleb, D. Williamson, P. Rasch, Description of the NCAR Community Climate Model (CCM3), *Tech. Rep. NCAR/TN-420+STR*, 152 pp., Natl. Cent for Atmos. Res., Boulder, Colo., 1996.

Kiehl, J. T., J. J. Hack, and J. W. Hurrell, The energy budget of the NCAR Community Climate Model: CCM3, *J. Clim.*, *11*, 1151–1178, 1998a.

Kiehl, J. T., J. J. Hack, G. B. Bonan, B. B. Boville, D. L. Williamson, and P. J. Rasch, The National Center for Atmospheric Research Community Climate Model: CCM3, *J. Clim.*, *11*, 1131–1149, 1998b.

Lubin, D., and D. A. Harper, Cloud radiative properties over the South Pole from AVHRR infrared data, *J. Clim.*, *9*, 3405–3418, 1996.

Manabe, S., and F. Möller, On the radiative equilibrium and heat balance of the atmosphere, *Mon. Weather Rev.*, *89*, 503–562, 1961.

Pinnock, S., and K. P. Shine, The effects of changes in HITRAN and uncertainties in the spectroscopy on infrared irradiance calculations, *J. Atmos. Sci.*, *55*, 1950–1964, 1998.

Pinto, J. O., J. A. Curry, and C. W. Fairall, Radiative characteristics of the Arctic atmosphere during spring as inferred from ground-based measurements, *J. Geophys. Res.*, *102*, 6941–6952, 1997.

Ramanathan, V., The role of ocean-atmosphere interactions in the CO_2 climate problem, *J. Atmos. Sci.*, *38*, 918–930, 1981.

Ramanathan, V., and P. Downey, A nonisothermal emissivity and absorptivity formulation for water vapor, *J. Geophys. Res.*, *91*, 8649–8666, 1986.

Raval, A., and V. Ramanathan, Observational determination of the greenhouse effect, *Nature*, *342*, 758–761, 1989.

Rind, D., E. W. Chiou, W. Chu, J. Larsen, S. Oltmans, J. Lerner, M. P. McCormick, and L. McMaster, Positive water vapor feedback in climate models confirmed by satellite data, *Nature*, *349*, 500–503, 1991.

Roberts, R. E., J. E. A. Salby, and L. M. Biberman, Infrared continuum absorption by atmospheric water vapor in the 8–12 μm window, *Appl. Opt.*, *15*, 2085–2090, 1976.

Rothman, L., (Ed.), *Proceedings of the 6th Biennial HITRAN Database Conference*, Harvard-Smithsonian Cent. for Astrophys., Cambridge, Mass., 2000.

Rothman, L. S., et al., The HITRAN molecular spectroscopic database and HAWKS (HITRAN Atmospheric Workstation): 1996 edition, *J. Quant. Spectrosc. Radiat. Transfer*, *60*, 665–710, 1998.

Schwarzkopf, M. D., and V. Ramaswamy, Radiative effects of CH_4, N_2O, halocarbons and the foreign-broadened H_2O continuum: A GCM experiment, *J. Geophys. Res.*, *104*, 9467–9488, 1999.

Soden, B., et al., An intercomparison of radiation codes for retrieving upper tropospheric humidity in the 6.3-μm band: A report from the First GVaP Workshop, *Bull. Am. Meteorol. Soc.*, *81*, 797–808, 2000.

Stephens, G. L., and T. J. Greenwald, The Earth's radiation budget and its relation to atmospheric hydrology, 1, Observations of the clear sky greenhouse effect, *J. Geophys. Res.*, *96*, 15,311–15,324, 1991.

Sundqvist, H., Parameterization of condensation and associated clouds in models for weather prediction and general circulation simulation, in *Physically-Based Modelling and Simulation of Climate and Climate Change*, vol. 1, edited by M. E. Schlesinger, pp. 433–461, Kluwer Acad., Norwell, Mass., 1988.

Tobin, D. C., et al., Downwelling spectral radiance observations at the SHEBA ice station: Water vapor continuum measurements from 17 to 26 μm, *J. Geophys. Res.*, *104*, 2081–2092, 1999.

Zhong, W., and J. D. Haigh, Improved broadband emissivity parameterization for water vapor cooling rate calculations, *J. Atmos. Sci.*, *52*, 124–138, 1995.

Zhong, W., and J. D. Haigh, The sensitivity of long-wave radiation fields and the response of a GCM to water-vapour continuum absorption, *Q. J. R. Meteorol. Soc.*, *125*, 1383–1406, 1999.

W. D. Collins, D. P. Edwards, and J. K. Hackney, National Center for Atmospheric Research, P. O. Box 3000, Boulder, CO 80307-3000, USA. (wcollins@ucar.edu; edwards@ucar.edu; hackney@ucar.edu)